

which are a significant characteristic of non-familial and some familial Parkinson's disease cases (Mizuno *et al.* 1998).

Eukaryotic cells coordinate the folding and glycosylation of secretory and membrane proteins in the endoplasmic reticulum. Various stresses leading to impairment of the endoplasmic reticulum and the production of mutant proteins cause the accumulation of unfolded proteins in the endoplasmic reticulum, culminating in cell death. Unfolded proteins accumulated in the endoplasmic reticulum are degraded by the ubiquitin-proteasome system (UPS). In this endoplasmic reticulum system, termed endoplasmic reticulum-associated degradation (ERAD), unfolded proteins are initially retrotranslocated from the endoplasmic reticulum to the cytosol through the translocon, polyubiquitylated by ubiquitin-conjugating enzyme (E2), ubiquitin ligase (E3), and other components, and degraded by the 26S proteasome (Hershko and Ciechanover 1998). E3 plays an important role in the ubiquitylation of unfolded proteins, and the RING finger domain of E3 mediates the transfer of ubiquitin from E2 to substrates (Zheng *et al.* 2000).

Parkin is an E3 that contains two RING finger domains; AR-JP-linked Parkin mutants have defective E3 activity. Parkin is up-regulated in response to endoplasmic reticulum stress and protects against cell death caused by such stress, suggesting that it is an E3 involved in ERAD. Parkin-associated endothelin receptor-like receptor (Pael-R) has been identified as a protein that interacts with Parkin; its accumulation leads to endoplasmic reticulum stress-induced cell death. Parkin ubiquitinates and promotes the degradation of insoluble Pael-R, resulting in the suppression of cell death (Imai *et al.* 2001). In other words, endoplasmic reticulum stress caused by the accumulation of unfolded Pael-R might be involved in AR-JP. Furthermore, it has been recently reported that Pael-R in Parkinson's disease is accumulated in the core of Lewy bodies (Murakami *et al.* 2004) and that selective dopaminergic neurodegeneration is caused by the ectopic expression of human Pael-R in the *Drosophila* brain (Yang *et al.* 2003).

It is known that in yeast, Hrd1p/Der3p is involved in ERAD. Hrd1p/Der3p is localized in the endoplasmic reticulum, contains the RING-finger domain at the C-terminus, and ubiquitinates substrates including HMG-CoA reductase (Hmg2p) (Gardner *et al.* 2000, 2001; Deak and Wolf 2001). Hrd3p is reported to regulate or stabilize Hrd1p (Plemper *et al.* 1999; Deak and Wolf 2001). Endoplasmic reticulum stress induces various components involved in ERAD, including Hrd1p as well as endoplasmic reticulum molecular chaperones, suggesting that ERAD involves the degradation of unfolded proteins in cooperation with endoplasmic reticulum chaperones (Friedlander *et al.* 2000; Travers *et al.* 2000). We previously reported that human HRD1 was identified and characterized as a human homolog of yeast Hrd1p (Kaneko *et al.* 2002). In that report, we demonstrated

that HRD1 possesses E3 activity, is induced during endoplasmic reticulum stress, and suppresses cell death caused by endoplasmic reticulum stress. Furthermore, human HRD1 is reportedly involved in the basal, and not the sterol-regulated, degradation of HMG-CoA reductase (Nadav *et al.* 2003; Kikkert *et al.* 2004) and is a pathogenic factor in rheumatoid arthritis (Amano *et al.* 2003).

The unfolded protein response (UPR) is required for the inhibition of further protein synthesis and the induction of endoplasmic reticulum chaperones, which reduce the number of unfolded proteins in the endoplasmic reticulum (Kaufman 1999, 2002). Transcription factor ATF6 is a transmembrane protein localized in the endoplasmic reticulum (Haze *et al.* 1999). Under endoplasmic reticulum stress, ATF6 is cleaved to release the N-terminal fragment on the cytosolic side of the membrane; it then enters the nucleus, acts as a transcription factor, and eventually activates endoplasmic reticulum chaperone gene transcription, which enhances protein folding (Haze *et al.* 1999; Ye *et al.* 2000; Shen *et al.* 2002). On the other hand, an endoplasmic reticulum-resident transmembrane protein IRE1, which possesses serine/threonine kinase and RNase domains, is dimerized and auto-phosphorylated during endoplasmic reticulum stress (Cox *et al.* 1993; Sidrauski and Walter 1997). Activated IRE1 splices XBP1 mRNA and then generates an active form of XBP1 (Yoshida *et al.* 2001).

Recent studies have demonstrated that Parkin knockout mice exhibit no significant change in either dopaminergic neurodegeneration or the accumulation of any Parkin substrates (Goldberg *et al.* 2003; Itier *et al.* 2003; Palacino *et al.* 2004; Von Coelln *et al.* 2004; Perez and Palmiter 2005; Periquet *et al.* 2005), suggesting that other unknown E3s can degrade accumulated proteins in the absence of Parkin. On the other hand, HRD1 apparently degrades a number of unfolded proteins as overexpressed HRD1 protects against endoplasmic reticulum stress-induced cell death. This study showed that human HRD1 was located in substantia nigra pars compacta (SNc) neurons in the mouse brain. Therefore, we hypothesized that HRD1 as well as Parkin ubiquitinates and degrades the unfolded Pael-R responsible for endoplasmic reticulum stress and protects against Pael-R-induced cell death. In addition, we investigated whether ATF6-induced UPR activation promotes the degradation of Pael-R and whether UPR-induced HRD1 expression is partially involved in this degradation.

## Materials and methods

### Constructs

The expression vector for human wild-type and truncated fragments of HRD1 was tagged with myc and polyhistidine (6 × His) epitopes at the C-terminus of the inserted sequence (pcDNA6; Invitrogen Corporation, Carlsbad, CA, USA). Human Pael-R (pcDNA3),

tagged with FLAG and 6 × His epitopes at the C-terminus, was a gift from Ryosuke Takahashi (RIKEN Brain Science Institute, Japan). The expression vector for wild-type human  $\alpha$ -synuclein, tagged with hemagglutinin and 6 × His epitopes at the C-terminus, was cloned into expression vector pcDNA3.1 (Invitrogen). The expression vector for the cleaved form of ATF6 (amino acid region 1–373 of ATF6 $\alpha$ ), tagged with hemagglutinin epitopes at the N-terminus was cloned into expression vector pCR3.1 (Invitrogen). The expression vector for RP-HRD1 fused at its N-terminus to glutathione S-transferase (GST) was cloned into the expression vector pGEX6p-1 (GE Healthcare Bio-Sciences, Piscataway, NJ, USA).

#### Affinity-purified antibodies, chemicals, and proteins

HRD1 polyclonal antibody against the KLH-conjugated synthetic peptide (C)-EDGEFPDAAELRRR, corresponding to amino acid residues 594–606 of human HRD1 protein, was recognized human and mouse HRD1 (a gift from Otsuka GEN Research Institute). We also purchased anti-HRD1 polyclonal antibody (C-term) from Abgent (San Diego, CA, USA). Anti-Pael-R polyclonal antibody was used as described (Imai *et al.* 2001). Anti-FLAG M2 polyclonal and HRP-conjugated M2 monoclonal antibodies, and M2 affinity gel were purchased from Sigma-Aldrich (St. Louis, MO, USA); anti-calreticulin polyclonal and anti-KDEL monoclonal antibodies were from Stressgen Biotechnologies Corporation (Ann Arbor, MI, USA); anti-myc monoclonal (9E10) antibody was from Oncogene Research Products (Cambridge, MA, USA); anti-caspase-3 (Asp175) polyclonal antibody was from Cell Signaling Technology Inc. (Danvers, MA, USA); anti-GST polyclonal (Z-5) and anti-hemagglutinin polyclonal (Y-11) antibodies were from Santa Cruz Biotechnology (Santa Cruz, CA, USA); MG132 was from the Peptide Institute (Osaka, Japan), and rabbit ubiquitin-activating enzyme (E1), GST-UbcH5c (E2), and GST-ubiquitin were from BostonBiochem (Cambridge, MA, USA). Horseradish peroxidase-conjugated anti-mouse IgG and anti-rabbit IgG (both from GE Healthcare Bio-sciences) were used as the secondary antibody. Bands were detected using the enhanced chemiluminescence (ECL) system (GE Healthcare Bio-Sciences).

#### Immunohistochemistry

Mouse brains were fixed in 4% paraformaldehyde, processed on a Tissue-Tek VIP (Sakura Finetek, Tokyo, Japan), and then embedded in paraffin. The brains were sectioned into 4- $\mu$ m-thick slices, mounted on silane-coated slides, and then subjected to heat treatment with 10 mM sodium citrate buffer (pH 6.0) in a pressure cooker for 3 min. Diaminobenzidine (DAB) immunostaining was performed using anti-HRD1 polyclonal antibody as the primary antibody (1 : 50 dilution), a peroxidase-labeled polymer-conjugated anti-rabbit antibody (Envision system; Dako, Glostrup, Denmark), and DAB as the substrate.

Immunofluorescence staining was stained with anti-HRD1 polyclonal antibody (1 : 20 dilution) and either anti-neuron-specific nuclear protein (NeuN; 1 : 100 dilution; Chemicon International, Temecula, CA, USA), anti-gial fibrillary acidic protein (GFAP; 1 : 100 dilution; Chemicon International), or anti-tyrosine hydroxylase (1 : 100 dilution; Chemicon International) monoclonal antibodies, and then with anti-mouse antibody conjugated with Alexa 546 and anti-rabbit antibody with Alexa 488 (Molecular Probes,

Eugene, OR, USA). Fluorescence images were acquired using a Zeiss LSM 510 confocal microscope (Carl Zeiss AG, Gottingen, Germany).

#### Immunocytochemistry

For the subcellular localization of HRD1 and Pael-R, COS-1 cells were transfected with HRD1-myc or a control vector (Mock) and Pael-R-FLAG using the calcium phosphate method. To visualize the effect of HRD1 degrading Pael-R, normal human embryonic kidney (HEK293) cells and those stably transfected with HRD1-myc and M-HRD1-myc were transfected with Pael-R-FLAG-pcDNA3 and DsRED-express-N1 vector (Promega, Madison, WI, USA) using LipofectAMINE 2000 (Invitrogen). At 36 h after transfection, the cells were fixed with methanol at  $-20^{\circ}\text{C}$ . The cells were then stained for the presence of proteins with appropriate primary antibodies, and then with anti-mouse antibody conjugated with Alexa 488 and/or anti-rabbit antibody with Alexa 594 (Molecular Probes). Fluorescence images were acquired using a Zeiss LSM 510 confocal microscope (Carl Zeiss AG, Gottingen, Germany).

#### Immunoprecipitation and western blotting

Transfected HEK293 cells were lysed in a lysis buffer [20 mM HEPES (pH 7.4), 120 mM NaCl, 5 mM EDTA, 10% glycerol, and 1% Triton X-100 with complete protease inhibitors (Roche Diagnostics K.K., Basel, Switzerland)]. Immunoprecipitation was carried out by incubating the supernatant with the indicated antibodies for 16 h and then with Protein G Sepharose Fast Flow (GE Healthcare Bio-sciences) for 1 h. For immunoprecipitation with an anti-FLAG antibody, the supernatant was incubated with anti-FLAG M2 affinity gel for 16 h. The immune complex was rinsed with a washing buffer [10 mM Tris-HCl (pH 7.5), 100 mM NaCl, 10% glycerol, and 0.2% Triton X-100].

#### Pulse-chase experiment

Neuro2a cells were transfected with Pael-R-FLAG and either a control vector, HRD1-myc or M-HRD1-myc. At 36 h after transfection, the cells were starved for 1 h in methionine/cysteine-free Dulbecco's modified Eagle's medium (DMEM; Sigma) containing 5% dialyzed fetal calf serum (FCS), and then labeled for 1 h at  $37^{\circ}\text{C}$  with 100  $\mu\text{Ci}/\text{mL}$  [ $^{35}\text{S}$ ]-methionine/cysteine (Redivue Promix L- $^{35}\text{S}$ ) *in vitro* cell labeling mix; GE Healthcare Bio-Sciences). The cells were then washed and incubated in DMEM containing 10% FCS for the indicated periods. The cell lysates were immunoprecipitated with the anti-FLAG antibody, subjected to sodium dodecyl sulfate-polyacrylamide gel electrophoresis (SDS-PAGE), and visualized using an imaging analyzer (BAS-2500, Fujifilm, Tokyo, Japan). The metabolically labeled Pael-R was quantified using Image Gauge software (Fujifilm).

#### Cell death assay

Normal HEK293 cells and those stably expressing HRD1-myc or M-HRD1-myc were transfected with a control vector or Pael-R-FLAG and incubated for 24 h. The cells were washed with phosphate-buffered saline (PBS) and then stained with crystal violet (0.1% crystal violet, WAKO Pure Chemical Industries, Osaka, Japan), and the wells washed with water and air-dried. The dye was eluted with water containing 0.5% SDS, and optical density was measured at 590 nm.

### *In vitro* ubiquitylation assay

RING-proline (RP)-HRD1-myc and Pael-R-FLAG were produced by T<sub>N</sub>T quick-coupled transcription/translation systems (Promega). Sixteen microliters of T<sub>N</sub>T reaction lysates producing RP-HRD1 or Pael-R-FLAG were mixed with other components including E1 (25 ng), E2 (GST-UbcH5c, 400 ng), and GST-ubiquitin (7 ng) in 100 µL of reaction buffer [40 mM Tris-HCl (pH 7.6), 5 mM MgCl<sub>2</sub>, 2 mM ATP, and 2 mM dithiothreitol (DTT)]. The reaction mixtures were incubated at 30°C for 90 min, immunoprecipitated with anti-FLAG antibody, subjected to SDS-PAGE, and analyzed by western blotting using the anti-GST polyclonal antibody.

### *In vitro* binding assay

RP-HRD1 was cloned into the pGEX 6p-1 vector (GE Healthcare Bio-Sciences). GST-RP-HRD1 and GST were expressed by culturing *Escherichia coli* DH5α with 0.5 mM isopropyl-β-D-thiogalactopyranoside (IPTG) for 4 h at 37°C. The cells were collected and lysed in a lysis buffer [10 mM HEPES (pH 7.4), 150 mM NaCl, 1 mM EGTA, 10%, 0.5% Triton X-100 with 1.5 mM phenylmethylsulfonyl fluoride (PMSF)]. The supernatants were mixed with glutathione-Sepharose 4B (GE Healthcare Bio-Sciences) for 16 h at 4°C. The beads were washed with lysis buffer and eluted with 50 mM Tris-HCl (pH 8.0) containing 10 mM reduced glutathione, and the eluted fraction dialyzed against PBS.

Equal amounts of purified GST or GST-RP-HRD1 were applied to glutathione Sepharose 4B in a binding buffer containing 50 mM Tris-HCl (pH 7.5), 150 mM NaCl, 1 mM EDTA, 0.25% gelatin, and 1% Triton X-100 at 4°C for 16 h, and then washed with the buffer. T<sub>N</sub>T reaction lysates producing <sup>35</sup>S-labeled Pael-R-FLAG were incubated with aliquots of GST- or GST-RP-HRD1-coupled glutathione-Sepharose 4B for 2 h at 4°C in the binding buffer. After extensive washing of the column with a washing buffer containing 10 mM Tris-HCl (pH 7.5), 150 mM NaCl, and 1% Triton X-100, the proteins recovered from the resin were subjected to SDS-PAGE followed by Coomassie blue staining and then visualized using an imaging analyzer (BAS-2500, Fujifilm).

### RNA interference

For HRD1 knockdown by RNA interference, siGENOME SMART-pools of four oligoduplexes targeted against HRD1 (M-007090-00; Dharmacon Research, Lafayette, CO, USA) were used. Small interfering RNA (siRNA) transfection was performed using 100 pmol of siRNA and 7.5 µL of LipofectAMINE 2000 reagent (Invitrogen) in 6 cm dishes.

## Results

### Localization of HRD1 and Pael-R in the murine brain and cellular endoplasmic reticulum

As HRD1 has been shown to be highly expressed in the human fetal brain by RT-PCR-ELISA (Nagase *et al.* 2001), we immunohistochemically examined where HRD1 is localized in the murine brain. DAB staining showed HRD1 expression was observed in SNC neurons, which are selectively degenerated in Parkinson's disease (Fig. 1a), as well as in pyramidal cells of the hippocampus and Purkinje

cells of the cerebellum (data not shown). Fluorescence staining using anti-NeuN and anti-GFAP antibodies showed that HRD1 was widely expressed in neuronal cells but not in glial cells (Fig. 1b). Furthermore, HRD1-immunoreactive cells were partially tyrosine hydroxylase-positive, indicating that HRD1 was expressed in dopaminergic neurons in the SNC (Fig. 1c). Thus, we hypothesized that HRD1 exists in the substantia nigra together with Pael-R as Pael-R is expressed in SNC dopaminergic neurons (Imai *et al.* 2001). To examine the subcellular localizations of HRD1 and Pael-R, expression vectors for HRD1-myc or the control vector (Mock) and Pael-R-FLAG were transfected into COS-1 cells. The localization of HRD1 (*green*) almost completely overlapped that of endogenous calreticulin (*red*) as revealed by an endoplasmic reticulum marker (Fig. 1d, lower). Pael-R (*red*) was widely localized in the endoplasmic reticulum as well as the cell surface and partially colocalized with HRD1 (*green*) in the endoplasmic reticulum (Fig. 1d, upper). Furthermore, endogenous HRD1 (*green*) was partially colocalized with Pael-R (*red*) in Pael-R-FLAG-expressing SH-SY5Y cells (Fig. 1e).

### HRD1 interacts with unfolded Pael-R

When Pael-R was overexpressed in HEK293 cells, Pael-R proteins migrated as high molecular mass broad smears (Fig. 2a, lane 2), suggesting that they had undergone covalent modifications (glycosylation, ubiquitylation, etc.) (Imai *et al.* 2001); however, in the transfection of Pael-R with hemagglutinin-Ub, the ubiquitylation of Pael-R was barely observed in the absence of proteasome inhibitor MG132 (Fig. 2a, lane 5). Therefore, we presumed that the high molecular mass broad smears observed were the result of the aggregate formation of detergent-insoluble Pael-R rather than ubiquitylated Pael-R. Next, we used the immunoprecipitation method to investigate whether HRD1 interacts with Pael-R. HRD1 protein was detected in anti-FLAG antibody immunoprecipitates from cells cotransfected with HRD1-myc and Pael-R-FLAG (Fig. 2b, lane 15). In addition, Pael-R protein was detected in immunoprecipitates with an anti-myc antibody (Fig. 2b, lane 3), indicating that HRD1 interacts with Pael-R.

Furthermore, we performed coimmunoprecipitation in SH-SY5Y cells that stably expressed Pael-R-FLAG. The endogenous HRD1 protein was detected in immunoprecipitates with overexpressed aggregated Pael-R (Fig. 2c, upper and lower, lane 4). To investigate the interaction between HRD1 and Pael-R under a wider range of physiological conditions, the endogenous proteins in dopaminergic neuroblastoma SH-SY5Y cells were coimmunoprecipitated with the anti-Pael-R antibody; however, HRD1 was not coimmunoprecipitated with Pael-R (Fig. 2d, lane 3) under normal conditions. As Pael-R is easily unfolded and becomes insoluble under endoplasmic reticulum stress, we investigated the interaction

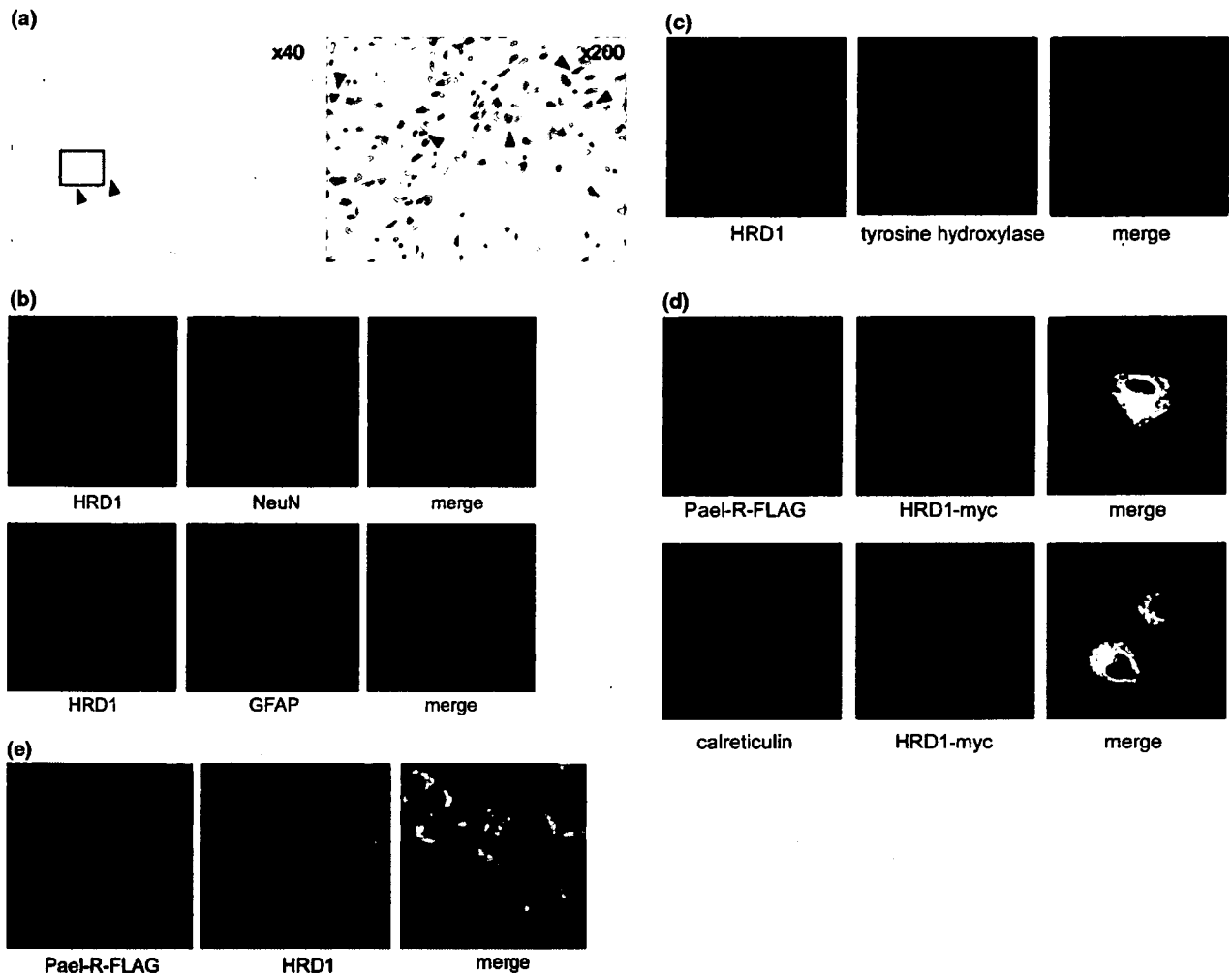


**Fig. 1** Brain distribution and subcellular localization of Pael-R and HRD1. (a) Immunolocalization of HRD1 in the coronal section of the murine brain. HRD1 localization was detected by DAB immunostaining using anti-HRD1 polyclonal antibody (pAb). The magnification of the box in the left panel ( $\times 40$ ) is part of the SNC, which is shown in the right panel ( $\times 200$ ). The arrowheads indicate the expression of HRD1. (b) Localization of HRD1 in neurons and glia. The *green* signal (HRD1) was obtained with anti-HRD1 pAb and anti-rabbit IgG Alexa 488-conjugated secondary Ab, while the *red* signal (Pael-R) was obtained with either anti-NeuN monoclonal Ab (mAb; dentate gyrus; upper panel) or anti-GFAP mAb (CA4; lower panel) and anti-mouse IgG Alexa 546-conjugated secondary Ab. (c) Colocalization of HRD1 and tyrosine hydroxylase in the SNC of the coronal section of murine brain. HRD1 was detected by anti-HRD1 pAb (*green*); tyrosine hydroxylase was detected by antityrosine hydroxylase mAb (*red*). *Yellow* indicates the co-expression of H-RD1 in the SNC. (d) Colocalization of HRD1

and Pael-R in the endoplasmic reticulum. COS-1 cells were transiently transfected with HRD1-myc and Pael-R-FLAG. At 24 h after transfection, the cells were fixed and subjected to indirect immunofluorescence staining with anti-myc mAb and anti-FLAG pAb, or anti-calreticulin pAb. The *green* signal (HRD1) was obtained with anti-mouse IgG Alexa 488-conjugated secondary Ab and the *red* signal (Pael-R or calreticulin) with anti-rabbit IgG Alexa 594-conjugated secondary Ab. Superimposing the two colors (merge) resulted in a *yellow* signal, indicating the colocalization of the two proteins. (e) Colocalization of HRD1 and Pael-R in the endoplasmic reticulum of SH-SY5Y cells. The SH-SY5Y cells expressing Pael-R-FLAG were fixed and subjected to indirect immunofluorescence staining with anti-FLAG mAb (*red*) and anti-HRD1 pAb (*green*). The *green* signal (HRD1) was obtained with anti-rabbit IgG Alexa 488-conjugated secondary Ab and the *red* signal (Pael-R) with anti-mouse IgG Alexa 594-conjugated secondary Ab.

between Pael-R and HRD1 in native SH-SY5Y cells under endoplasmic reticulum stress. HRD1 was precipitated with Pael-R that tends to exist in an unfolded state under endoplasmic reticulum stress conditions (Fig. 2d, lane 4); this indicates that HRD1 interacts with the unfolded form of Pael-R.

#### HRD1 interacts with and ubiquitinates Pael-R through the proline-rich region

To investigate which HRD1 region interacts with Pael-R, a series of HRD1 mutants was prepared (Fig. 3a). HEK293 cells were transiently transfected with Pael-R-FLAG along with an empty vector (Mock), wild-type (wt)-HRD1-myc,

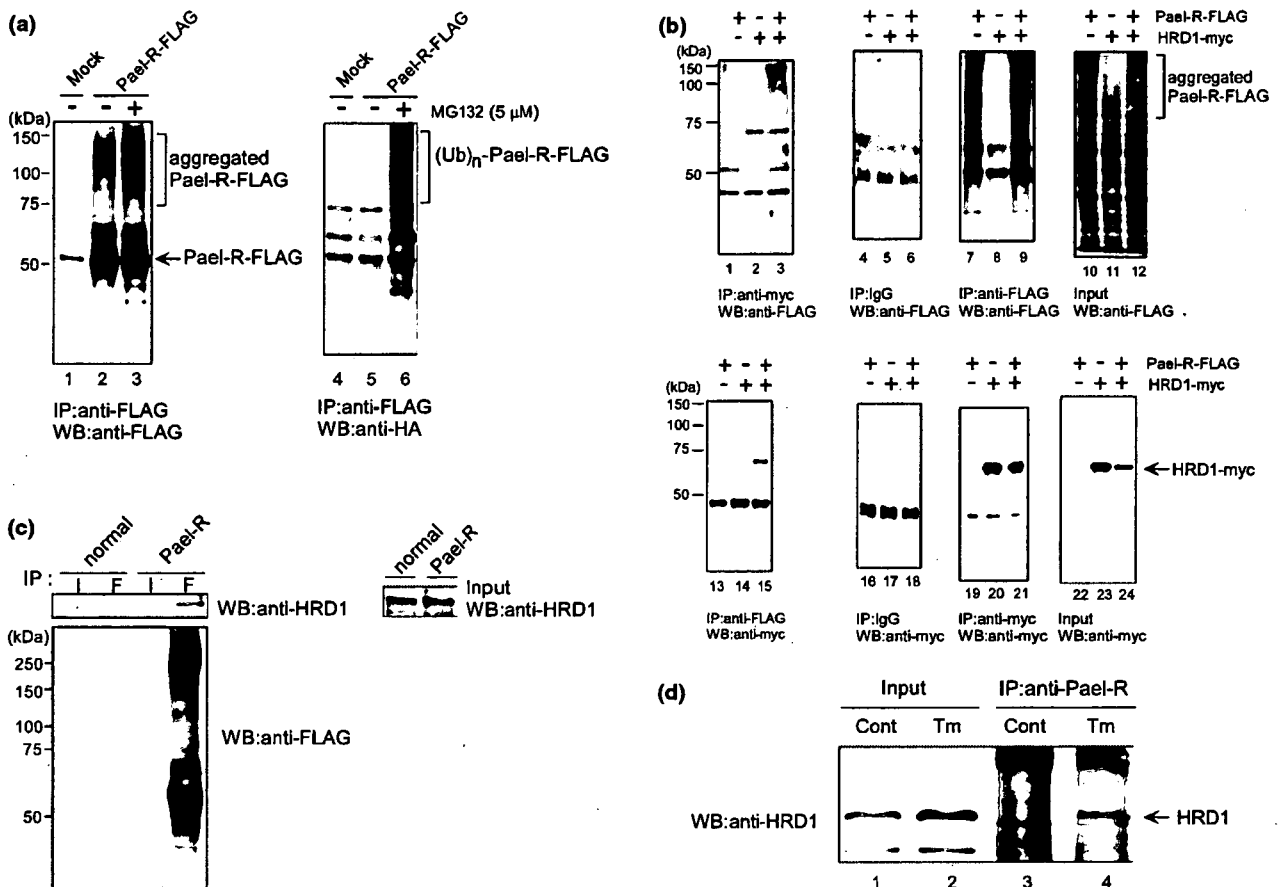


**Fig. 2** Interaction of HRD1 with aggregated Pael-R. (a) Pael-R tends to exist in an aggregated form. HEK293 cells were transiently transfected with hemagglutinin-ubiquitin and an empty vector (Mock) or Pael-R-FLAG and incubated in the presence or absence of 5  $\mu$ M MG132 (proteasome inhibitor). Equal amounts of proteins were immunoprecipitated with anti-FLAG mAb, and the immune complex was then analyzed by western blotting using anti-FLAG mAb (left) or anti-hemagglutinin pAb (right). (b) Interaction of Pael-R with HRD1 in HEK293 cells. HRD1 and Pael-R were coimmunoprecipitated in HEK293 cells transiently transfected with or without Pael-R-FLAG and HRD1-myc. At 48 h after transfection, the total cell lysates (Input) were analyzed by western blotting to check the expression of Pael-R and HRD1 proteins. Equal amounts of the proteins were immunoprecipitated with normal mouse IgG, anti-myc mAb, or anti-FLAG mAb. The immune complex was lysed in SDS sample buffer, resolved by SDS-PAGE, and analyzed by western blotting using anti-myc mAb or anti-FLAG mAb. (c) Endogenous HRD1 interacts with Pael-R in neuroblastoma SH-SY5Y cells stably expressing Pael-R-FLAG. The total cell lysates that stably expressed Pael-R-FLAG in neuroblastoma SH-SY5Y cells were analyzed by western blotting using anti-HRD1 pAb (Input, right panel). Equal amounts of the proteins were immunoprecipitated with normal mouse IgG (I) or anti-FLAG mAb (F), and the immune complex was then analyzed by western blotting using anti-HRD1 pAb (left panel, upper) or anti-FLAG mAb (right panel, lower). (d) Endogenous interaction of HRD1 with Pael-R in tunicamycin-treated neuroblastoma SH-SY5Y cells. The SH-SY5Y cells were either untreated (control) or treated (tunicamycin) with 2.5  $\mu$ g/mL tunicamycin for 24 h. The total cell lysates (Input, lanes 1 and 2) were analyzed by western blotting to check the expression of HRD1 proteins. Equal amounts of proteins were immunoprecipitated with anti-Pael-R pAb. The immune complex was analyzed by western blotting by using anti-HRD1 pAb (IP, lanes 3 and 4; Abgent).

FLAG mAb. (c) Endogenous HRD1 interacts with Pael-R in neuroblastoma SH-SY5Y cells stably expressing Pael-R-FLAG. The total cell lysates that stably expressed Pael-R-FLAG in neuroblastoma SH-SY5Y cells were analyzed by western blotting using anti-HRD1 pAb (Input, right panel). Equal amounts of the proteins were immunoprecipitated with normal mouse IgG (I) or anti-FLAG mAb (F), and the immune complex was then analyzed by western blotting using anti-HRD1 pAb (left panel, upper) or anti-FLAG mAb (right panel, lower). (d) Endogenous interaction of HRD1 with Pael-R in tunicamycin-treated neuroblastoma SH-SY5Y cells. The SH-SY5Y cells were either untreated (control) or treated (tunicamycin) with 2.5  $\mu$ g/mL tunicamycin for 24 h. The total cell lysates (Input, lanes 1 and 2) were analyzed by western blotting to check the expression of HRD1 proteins. Equal amounts of proteins were immunoprecipitated with anti-Pael-R pAb. The immune complex was analyzed by western blotting by using anti-HRD1 pAb (IP, lanes 3 and 4; Abgent).

membrane (M)-HRD1  $\Delta$ membrane ( $\Delta$ M)-HRD1-myc, or membrane-RING (MR)-HRD1-myc. Wt-HRD1 and  $\Delta$ M-HRD1 were detected in immunoprecipitates with anti-FLAG, whereas (M)-HRD1 and (MR)-HRD1 were not detected (Fig. 3b, upper, lanes 3, 5), suggesting that HRD1 requires a proline-rich region for association with Pael-R. We examined whether Pael-R interacts with the proline-rich region of HRD1 *in vitro* (Fig. 4a). In an *in vitro* GST pull-down assay, RP-HRD1 bound to both the native and aggregated forms of

Pael-R (Fig. 4a, upper, lane 5). Thus, HRD1 may directly interact with Pael-R through the proline-rich region. We then evaluated whether HRD1 ubiquitinates Pael-R through its E3 activity *in vitro*. Using RP-HRD1-myc and Pael-R-FLAG generated by *in vitro* translations (Fig. 4b), we examined whether Pael-R is ubiquitylated by RP-HRD1 *in vitro*. Recombinant E2 Ubch5c was used in this assay as HRD1 is shown to be ubiquitylated by Ubch5c *in vitro* (Nadav *et al.* 2003; Kikkert *et al.* 2004). *In vitro* transcrip-

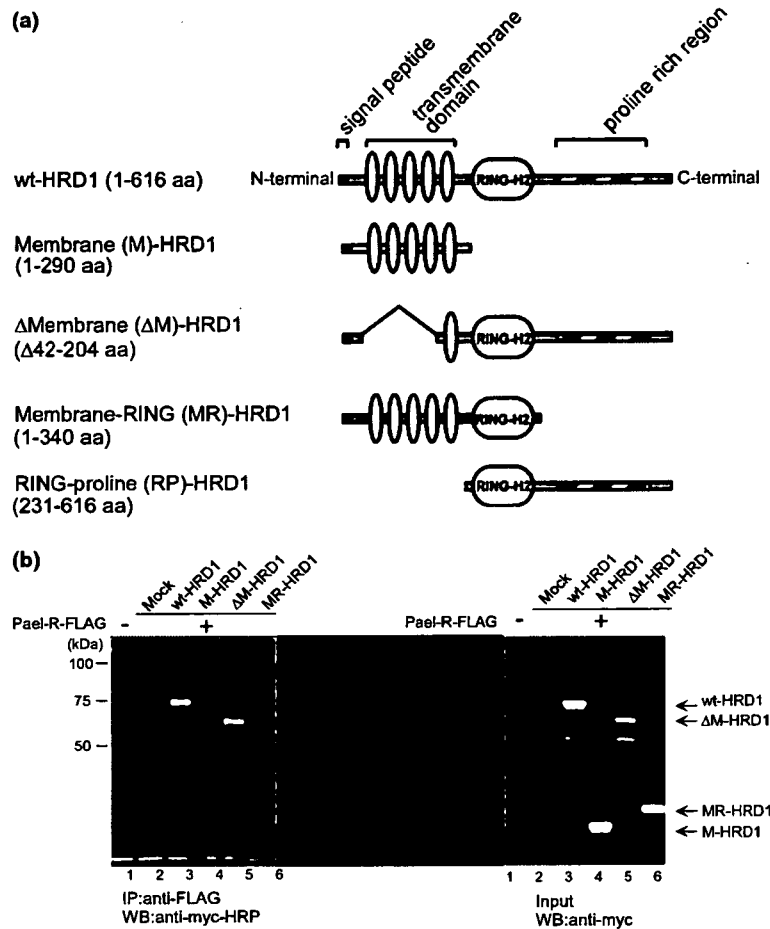


**Fig. 3** Interaction of Pael-R with HRD1 and its mutants. (a) Schematic representation of the HRD1 constructs. The panel diagrammatically represents wild-type HRD1 and a variety of HRD1 mutants used to determine the Pael-R binding domain. Numbers in parentheses indicate the corresponding amino acid residues of HRD1. (b) Coimmunoprecipitation of Pael-R and a variety of HRD1 mutants. Coimmunoprecipitation was performed in HEK293 cells transiently

transfected with Pael-R-FLAG and an empty vector (Mock), wild-type (wt)-HRD1-myc, membrane (M)-HRD1-myc, Δmembrane (ΔM)-HRD1-myc or membrane-RING (MR)-HRD1-myc. At 48 h after transfection, the total cell lysates (Input) were analyzed by western blotting using antimyc mAb (right). Equal amounts of the proteins were immunoprecipitated with anti-FLAG mAb, and the immune complex was then analyzed by western blotting using antimyc mAb (left).

tion/translation reaction lysates containing RP-HRD1 and Pael-R were incubated with other components including E1 (rabbit), E2 (GST-UbcH5c), and GST-ubiquitin. Pael-R-FLAG proteins were ubiquitylated only in the presence of RP-HRD1 along with all other components (Fig. 4c, lane 6), indicating that HRD1 directly interacts with and ubiquitinates Pael-R.

#### HRD1 degrades unfolded Pael-R

We investigated whether HRD1 accelerates Pael-R degradation via the UPS. Normal HEK293 cells and those stably expressing wt-HRD1 or M-HRD1 were transiently transfected with Pael-R-FLAG. Equal amounts of proteins were immunoprecipitated with anti-FLAG monoclonal antibody and subjected to western blotting. Pael-R and its high molecular mass broad smears were markedly decreased in

wt-HRD1-expressing cells (Fig. 5a, first panel, lanes 5, 6). MG132 inhibited the decrease of Pael-R protein (Fig. 5a, first panel, lane 7), indicating that HRD1 promoted the degradation of Pael-R via the UPS. In contrast, Pael-R was not degraded by M-HRD1, which has no RING-finger domain and lacks E3 activity (Fig. 5a, first panel, lanes 8, 9). To confirm that these results were not caused by a decrease in the transfection or transcription efficiency of Pael-R, the expression level of Pael-R mRNA was examined by RT-PCR using the total RNA of the cells used in western blotting. In each clone, the expression levels of transfected Pael-R were almost equal (Fig. 5a, third panel); furthermore, another clone stably expressing wt-HRD1 degraded Pael-R (data not shown).

To immunocytochemically visualize the degradation of Pael-R by HRD1, normal HEK293 cells and those stably



**Fig. 4** HRD1 ubiquitinates Pael-R *in vitro*. (a) Coimmunoprecipitation of Pael-R with RING-proline (RP)-HRD1 *in vitro*. GST-fused RP-HRD1 or GST alone was bound to glutathione beads incubated with [ $^{35}$ S]-labeled Pael-R generated by an *in vitro* transcription/translation system. After extensive washing, the protein-bound beads were resolved by SDS-PAGE followed by Coomassie blue staining (lower), and detected by autoradiography (upper). (b) Protein products of Pael-R and RP-HRD1. Western blotting analysis of the components used for *in vitro* ubiquitylation assays. RP-HRD1-myc and Pael-R-FLAG were produced by a  $T_NT$  quick-coupled transcription/translation system.  $T_NT$  reaction lysates containing RP-HRD1 were analyzed by

western blotting using anti-myc mAb (left), whereas  $T_NT$  reaction lysates containing Pael-R were immunoprecipitated with anti-FLAG mAb. The immune complex was then analyzed by western blotting using anti-FLAG mAb (right). (c) *In vitro* ubiquitylation assay. Western blotting analysis of the *in vitro* ubiquitylation reactions mediated by HRD1 with anti-GST pAb.  $T_NT$  reaction lysates containing RP-HRD1 and Pael-R were mixed with other components including E1 (rabbit), E2 (GST-UbcH5c), or GST-ubiquitin in the reaction buffer. The reaction lysates were then incubated at 30°C for 90 min, immunoprecipitated with anti-FLAG mAb, and analyzed by western blotting using anti-GST pAb.

expressing wt-HRD1 or M-HRD1 were transfected with Pael-R-FLAG and DsRED, a red fluorescent protein. The amount of Pael-R-FLAG protein decreased in cells expressing wt-HRD1-myc compared with control cells, whereas the amount of Pael-R-FLAG protein in cells expressing M-HRD1-myc and in control cells was similar (Fig. 5b, upper, green). The red signals (lower panels) were DsRED proteins cotransfected with Pael-R-FLAG for use as transfection controls. These results indicate that HRD1 degrades Pael-R by its E3 activity.

Next, the degradation of Pael-R by HRD1 was examined by performing a pulse-chase experiment. The levels of  $^{35}$ S-labeled Pael-R were plotted relative to the amount present at time 0 (Fig. 5c). Following a 3 h chase, 54.4% and 52.0% of *de novo* synthesized Pael-R remained in cells transfected with Mock and M-HRD1, respectively. In contrast, Pael-R degradation in HRD1-transfected cells was accelerated such that at 3 h, 28.7% of proteins remained, indicating that

HRD1 accelerates the degradation of newly synthesized Pael-R protein.

Furthermore, to investigate whether HRD1 is involved in the physiological degradation of Pael-R, we examined the effect of HRD1 suppression by siRNA on Pael-R accumulation in SH-SY5Y cells stably expressing Pael-R-FLAG. The amount of the aggregated form of Pael-R was increased by the suppression of HRD1 expression (Fig. 5d, upper, lane 2) whereas the native form was not affected markedly; thus, it is possible that endogenous HRD1 preferentially degrades aggregated Pael-R but not native Pael-R.

$\alpha$ -Synuclein is a component of Lewy bodies in Parkinson's disease (Trojanowski *et al.* 1998), and a 22-kD glycosylated form of  $\alpha$ -synuclein is reported to be ubiquitylated by Parkin (Shimura *et al.* 2001), and is ubiquitylated when overexpressed in cells (Imai *et al.* 2000). Unfolded  $\alpha$ -synuclein can be degraded by the 20S proteasome *in vitro* (Tofaris *et al.* 2001). We examined whether  $\alpha$ -synuclein, like Pael-R, is a

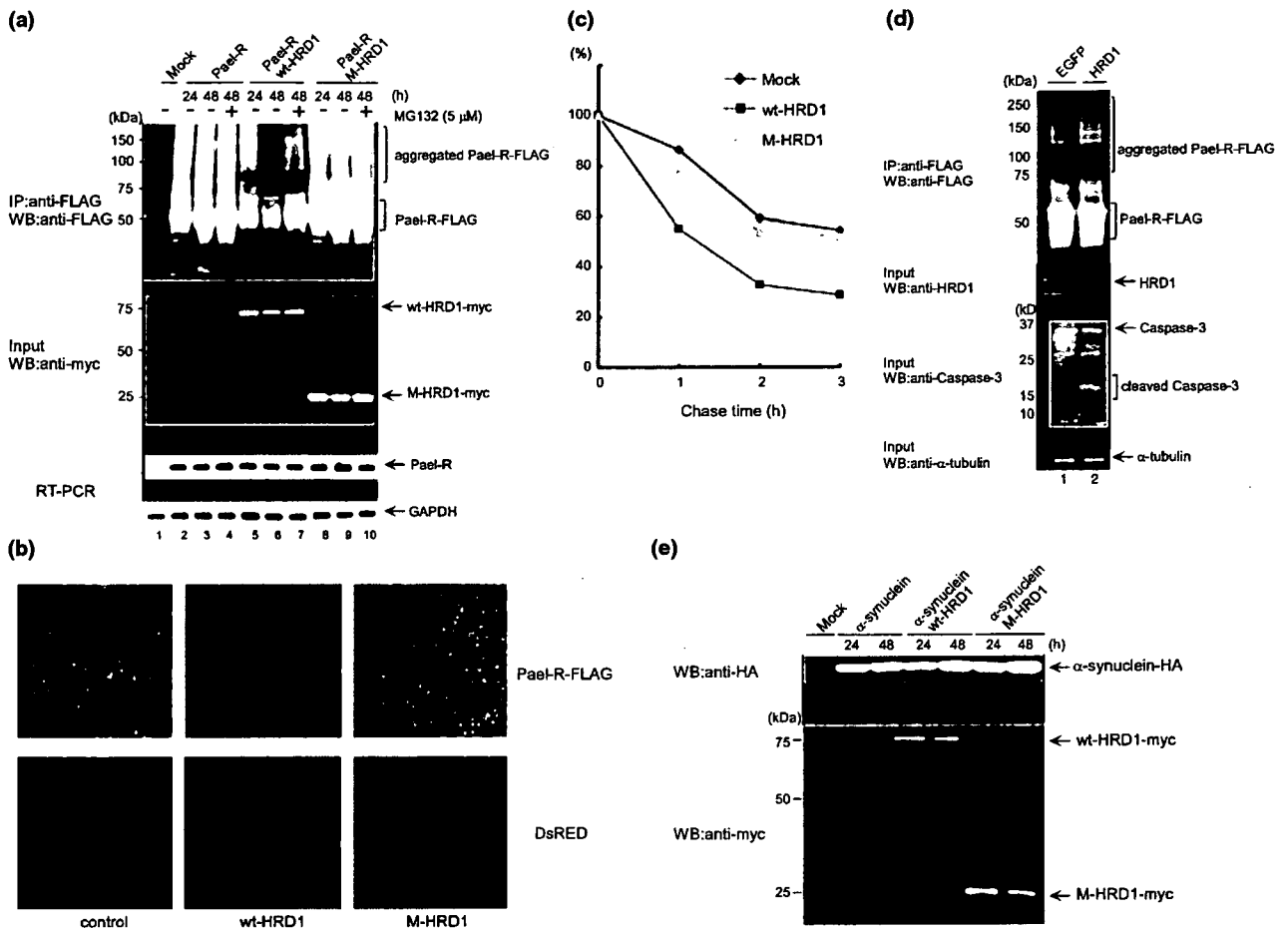


**Fig. 5** Degradation of Pael-R by HRD1. (a) HEK293 cells stably expressing wt-HRD1 or M-HRD1 were transiently transfected with Pael-R-FLAG and incubated for the indicated periods in the presence or absence of 5 μM MG132, which was added 12 h before cell harvest. The total cell lysates (Input) were analyzed by western blotting using anti-myc mAb (middle). Equal amounts of the proteins were immunoprecipitated with anti-FLAG mAb, and the immune complex was then analyzed by western blotting using anti-FLAG mAb (upper). The total RNA of the cells used in western blotting was prepared and subjected to RT-PCR (lower). (b) HEK293 cells stably expressing wt-HRD1 or M-HRD1 were transiently transfected with Pael-R-FLAG and DsRED (red fluorescent protein). At 36 h after transfection, the cells were fixed and subjected to indirect immunofluorescence staining with anti-FLAG mAb (upper). The *green* signal (Pael-R) was obtained with anti-mouse IgG Alexa 488-conjugated secondary Ab while the *red* signal (lower) shows DsRED proteins used as a transfection control. (c) Pulse-chase assay. Neuro2a cells were transiently transfected with Pael-R-FLAG and an empty vector (Mock), wt-HRD1, or M-HRD1. At 36 h after transfection, cells were pulse-labeled with [<sup>35</sup>S]-methionine/cysteine and chased for the indicated periods. Equal amounts of [<sup>35</sup>S]-

labeled Pael-R and M-HRD1 were immunoprecipitated with anti-FLAG mAb; the immune complex was then lysed in SDS sample buffer, resolved by SDS-PAGE, detected by autoradiography, and quantified by phosphorimaging. The levels of [<sup>35</sup>S]-labeled Pael-R are plotted relative to the amount present at time 0. (d) Induction of aggregated Pael-R accumulation and caspase activation by inhibition of HRD1 expression. SH-SY5Y cells stably expressing Pael-R-FLAG were transiently transfected with the siRNA of enhanced green fluorescent protein (EGFP, control) or HRD1, and incubated for 72 h. The total cell lysates were analyzed by western blotting using anti-HRD1 pAb (2nd panel), anti-caspase-3 pAb (3rd panel), and anti-α-tubulin mAb (5th panel). Equal amounts of the proteins were immunoprecipitated with anti-FLAG mAb, and the immune complex was then analyzed by western blotting using anti-FLAG mAb (1st panel). (e) HRD1 did not degrade α-synuclein. HEK293 cells stably expressing wt-HRD1 or M-HRD1 were transiently transfected with α-synuclein-hemagglutinin and incubated for the indicated periods. The total cell lysates were analyzed by western blotting using anti-hemagglutinin pAb (upper) or anti-myc mAb (lower).

substrate of HRD1. Normal HEK293 cells and those stably expressing wt- or M-HRD1 were transiently transfected with α-synuclein-hemagglutinin. The protein levels of α-synuclein were not changed by HRD1 (Fig. 5e, upper), indicating that α-synuclein is not a substrate of HRD1.

**HRD1 suppresses Pael-R-induced cell death**

The accumulation of Pael-R causes endoplasmic reticulum stress and subsequent cell death. We investigated whether HRD1 suppresses Pael-R-induced cell death. Normal HEK293 cells and those stably expressing wt- or M-HRD1



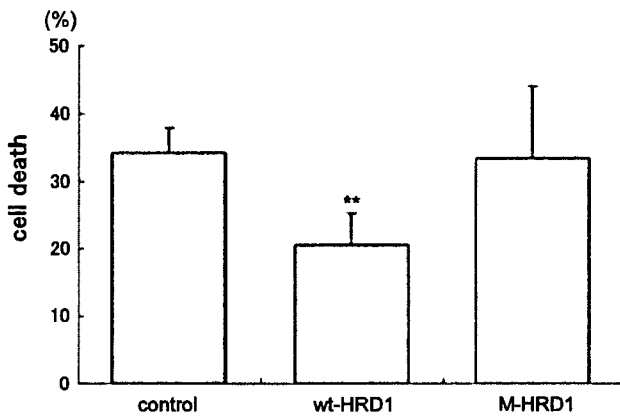


**Fig. 6** HRD1 protects against Pael-R-induced cell death. HEK293 cells (control) and HEK 293 cells stably expressing wt-HRD1 or M-HRD1 were transiently transfected with a control vector (Mock) or Pael-R-FLAG and incubated for 24 h. The cells were washed with PBS and then stained with crystal violet (0.1%) for 20 min, and the wells were washed with water and air-dried. The dye was eluted with water containing 0.5% SDS for 20 min, and the optical density at 590 nm was measured. The percentage of cell death was calculated as follows:  $100 - [(OD \text{ for assay}/OD \text{ for control well}) \times 100]$ . The results obtained from each cell transfected with Pael-R-FLAG were compared with those obtained from cells transfected with Mock. The results are expressed as the means  $\pm$  SD (three independent experiments in duplicate). Statistical analysis was performed with Student's *t*-test (\*\**p* < 0.01, vs. normal).

were transiently transfected with a control vector (Mock) or Pael-R-FLAG and incubated for 24 h. The cell death of HEK293 was compared with that of cells transfected with the control vector. The crystal violet assay showed that wt-HRD1-expressing cells were more resistant to Pael-R over-expression than control and M-HRD1 cells (control, 34.3%; wt-HRD1, 20.8%; M-HRD1, 33.4%) (Fig. 6). Furthermore, we found that the accumulation of aggregated Pael-R induced by the repression of HRD1 in SH-SY5Y cells that stably expressed Pael-R-FLAG promoted a decrease in pro-caspase-3 and an increase in cleaved caspase-3 (Fig. 5d, third panel, lane 2), which indicates the activation of caspase-3 and subsequent apoptosis. These results indicate that HRD1 suppresses apoptosis induced by Pael-R accumulation.

**Involvement of HRD1 in the degradation of Pael-R induced by ATF6**

We found that ATF6 induced the expression of HRD1 (Kaneko *et al.* 2002; unpublished data). As ATF6-mediated UPR possibly induces a number of ERAD genes, we speculated that the degradation of Pael-R is promoted by ATF6. HEK293 cells were transiently transfected with Pael-R-FLAG and either an empty vector (Mock) or hemagglutinin-ATF6 (1–373; cytoplasmic domain worked as a transcription factor), and incubated for 48 h in the presence or absence of MG132. The amount of both native and aggregated Pael-R decreased in cells expressing ATF6

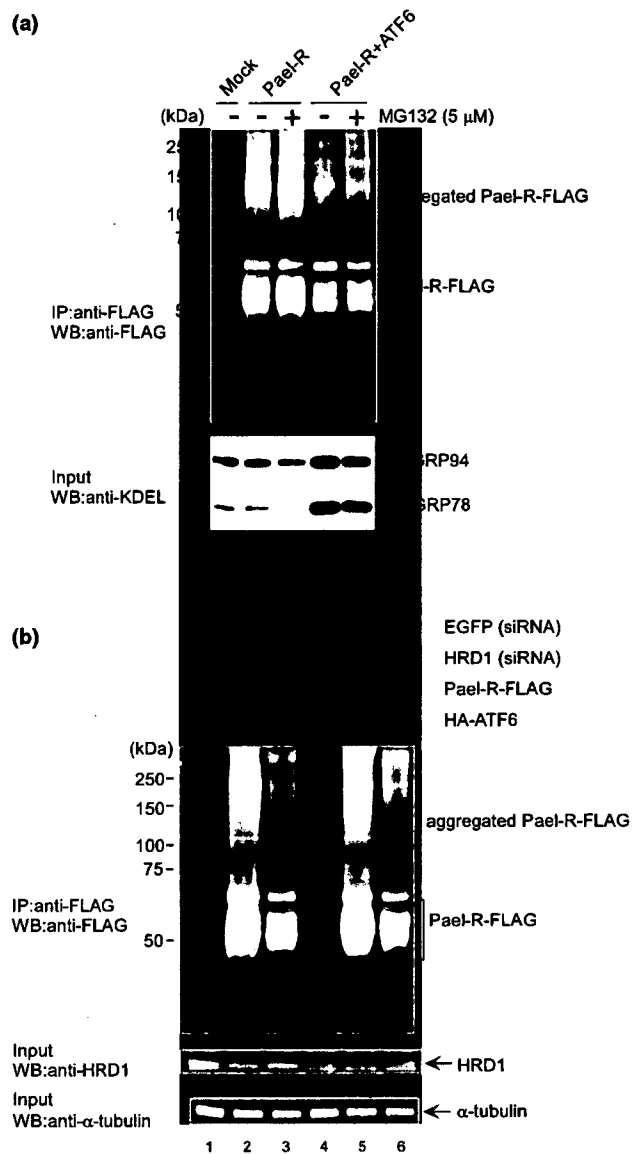


**Fig. 7** Degradation of Pael-R promoted by ATF6. (a) HEK293 cells were transiently transfected with an empty vector (Mock) or Pael-R-FLAG with or without hemagglutinin-ATF6 (cleaved form); they were incubated for 48 h in the presence or absence of 5 μM MG132 (12 h incubation). The total cell lysates (Input) were analyzed by western blotting using anti-KDEL mAb (lower). Equal amounts of the proteins were immunoprecipitated with anti-FLAG mAb, and then analyzed by western blotting using anti-FLAG mAb (upper). (b) Involvement of HRD1 in ATF6-mediated Pael-R degradation. HEK293 cells were transiently transfected with Pael-R-FLAG and hemagglutinin-ATF6 (cleaved form) and siRNA of EGFP (control) or HRD1 and incubated for 30 h. The total cell lysates (Input) were analyzed by western blotting using anti-HRD1 pAb (middle) or anti-α-tubulin mAb (lower). Equal amounts of the proteins were immunoprecipitated with anti-FLAG mAb, and the immune complex was then analyzed by western blotting using anti-FLAG mAb (upper).

(Fig. 7a, upper, lane 4); moreover, MG132 inhibited the decrease in Pael-R protein by ATF6 overexpression (Fig. 7a, upper, lane 5). The increased expression of glucose-regulated proteins GRP78 and GRP94 indicates the induction of UPR by ATF6 (Fig. 7a, lower, lanes 4, 5). These results indicate that the up-regulation of UPR by ATF6 leads to the degradation of Pael-R proteins via the UPS; however, it is not known which proteins induced by ATF6 are involved in this degradation.

To determine whether HRD1 is involved in the degradation of Pael-R induced by UPR up-regulation, we investigated the effect of HRD1 suppression by siRNA on degradation. HEK293 cells were transiently transfected with Pael-R-FLAG, hemagglutinin-ATF6, and either green fluorescent protein (GFP) (siRNA) or HRD1 (siRNA). ATF6 induced HRD1 expression (Fig. 7B, lower, lane 3), whereas HRD1 repression partially suppressed the ATF6-induced decrease in the number of Pael-R aggregates, but not the amount of the native form (Fig. 7b, upper, lane 6), suggesting that UPR-induced HRD1 preferentially promotes the degradation of unfolded Pael-R.

## Discussion

In this report, we found that HRD1 was expressed in the dopaminergic neurons of the SNC, colocalized with Pael-R in the endoplasmic reticulum, and directly interacted with Pael-R at the proline-rich region of HRD1. We showed that HRD1 promoted the ubiquitylation and degradation of Pael-R; additionally, the activation of UPR by ATF6 induced Pael-R degradation, which partially depends on HRD1.

First, we found that HRD1 was locally expressed in SNC neurons, including dopaminergic neurons, of the murine brain. Pael-R is reportedly expressed in SNC neurons, implying that HRD1 and Pael-R are colocalized in dopaminergic neurons in the SNC. Parkin, an E3, is up-regulated in response to endoplasmic reticulum stress and protects cells via ERAD from endoplasmic reticulum stress-induced apoptosis (Imai *et al.* 2000). Pael-R accumulates in the brains of AR-JP patients and induces endoplasmic reticulum stress, possibly because of Parkin mutation (Imai *et al.* 2001). Furthermore, it has been reported that Pael-R overexpression causes the selective degeneration of dopaminergic neurons in *Drosophila* and that the coexpression of human Parkin suppresses Pael-R toxicity by degrading Pael-R. It has also been reported that interference in endogenous *Drosophila* Parkin functions enhances Pael-R toxicity (Yang *et al.* 2003). On the other hand, we previously reported that human HRD1 is up-regulated in response to endoplasmic reticulum stress. It possesses E3 activity and protects against endoplasmic reticulum stress-induced cell death (Kaneko *et al.* 2002), suggesting that HRD1 can degrade protein substrates accumulated during endoplasmic reticulum stress. There is, however, little information regarding these sub-

strates, with the exception of CD-3 $\alpha$  and TCR- $\alpha$ , and HMG-CoA reductase (Kikkert *et al.* 2004). We showed that HRD1 was colocalized in the endoplasmic reticulum with Pael-R and they interacted at endogenous levels as well as overexpression levels. We therefore hypothesized that HRD1, like Parkin, may degrade Pael-R and suppress cell death caused by Pael-R accumulation.

We found that endogenous HRD1 interacted with not only overexpressed Pael-R but also endogenous Pael-R under endoplasmic reticulum stress conditions. Pael-R tends to exist in an unfolded state when it is overexpressed or when subjected to endoplasmic reticulum stress; therefore, it is likely that HRD1 preferentially interacts with the unfolded form of Pael-R but not with the normally folded form. Therefore, it can be speculated that unfolded Pael-R is recognized by acceptors of terminally misfolded glycoproteins, such as endoplasmic reticulum degradation-enhancing alpha-mannosidase-like protein (EDE), and is destined to be eliminated from the endoplasmic reticulum (Molinari *et al.* 2003; Oda *et al.* 2003); HRD1 then binds to Pael-R passing through the translocon in the endoplasmic reticulum membrane by its proline-rich region and ubiquitinates the unfolded form of Pael-R. If this is true, it is unlikely that HRD1 directly associates with and ubiquitinates native Pael-R on the endoplasmic reticulum membrane without mediation of the translocon.

On the other hand, we showed that the high molecular mass broad smears of Pael-R mostly comprised not ubiquitylated forms, but possibly glycosylated or aggregated forms, as previously reported (Imai *et al.* 2001). The inhibition of HRD1 expression by siRNA induced the accumulation of smears and the activation of caspase-3. Therefore, it is likely that HRD1 preferentially ubiquitinates and degrades unfolded Pael-R to prevent the accumulation of aggregated Pael-R that leads to endoplasmic reticulum stress-induced apoptosis.

We further showed that HRD1 interacted with Pael-R at its proline-rich region and ubiquitylated Pael-R *in vitro*, indicating direct interaction between the proline-rich region of HRD1 and Pael-R. Yeast Hrd1p has no proline-rich region, whereas human HRD1 contains a proline-rich region similar to that seen in the Cbl family of ubiquitin ligases (Fujita *et al.* 2002). It has been reported that the proline-rich region is essential for protein-protein interaction and that the RING-finger and proline-rich regions are sufficient for the binding and ubiquitylation of substrates (Fang *et al.* 2001). Therefore, human HRD1 appears to interact with substrates at the proline-rich region and ubiquitinates the substrates at the RING-finger domain. On the other hand, Hrd1p degrades Hmg2p, one of the yeast isozymes of HMG-CoA reductase, despite the lack of a proline-rich region (Gardner *et al.* 2000). Thus, we propose that in the course of evolution, human HRD1 acquired a proline-rich region to interact with and ubiquitinate a variety of substrates; whether other

substrates are bound to the proline-rich region remains to be determined.

We investigated whether  $\alpha$ -synuclein is a substrate of HRD1. An  $\alpha$ -synuclein mutant (Ala53Thr or Ala30Pro) has been reported in the brain of Parkinson's disease patients, promoting protofibril formation relative to wild-type  $\alpha$ -synuclein (Conway *et al.* 2000). Parkin ubiquitinates the *O*-glycosylated form ( $\alpha$ Sp22) (Shimura *et al.* 2001) and suppresses the toxicity of normal or pathogenic alpha-synuclein (Petrucci *et al.* 2002; Yang *et al.* 2003; Lo Bianco *et al.* 2004; Haywood and Staveley 2004). HRD1 did not degrade wild-type  $\alpha$ -synuclein, probably due to the different localization or binding ability of HRD1 and  $\alpha$ -synuclein; however, whether HRD1 degrades  $\alpha$ -synuclein mutants or the *O*-glycosylated form remains to be clarified. On the other hand, Hrd3p, another UPR-inducible ERAD protein, has been reported to interact with Hrd1p and mediate the regulation of Hrd1p stability and activity in yeast (Gardner *et al.* 2000). We have identified SEL1 as a candidate human homolog of Hrd3p and have found that SEL1 interacted with human HRD1 (data not shown). We have further found that HRD1 did not degrade SEL1 despite this interaction; rather, the amount of SEL1 increased in the presence of HRD1 (data not shown). Based on these observations, we speculate that HRD1 specifically increases the degradation of proteins.

When unfolded proteins accumulate in the endoplasmic reticulum, the UPR is activated by ATF6 and IRE1, resulting in the induction of several endoplasmic reticulum chaperones and ERAD components (Travers *et al.* 2000; Lee *et al.* 2003). Therefore, we hypothesized that ATF6 promotes the degradation of Pael-R by inducing UPR genes including HRD1, although ATF6 can induce a variety of genes in addition to HRD1. Interestingly, ATF6 induced the degradation of both aggregated and unaggregated Pael-R, whereas the suppression of ATF6-induced HRD1 expression by siRNA caused an increase in the aggregated form. Thus, it is likely that endogenous HRD1 preferentially recognizes and degrades the unfolded forms of Pael-R. Based on these results, we propose that after the accumulation of unfolded Pael-R due to stress or Parkin mutation, ATF6 and/or IRE1-XBP1 pathways are activated and induce UPR genes including HRD1; this promotes the folding or degradation of unfolded Pael-R to prevent unfolded Pael-R-induced cell death (Fig. 8).

It has been reported that Parkin knockout mice exhibit little change in movement ability or the neurons of the substantia nigra (Itier *et al.* 2003; Goldberg *et al.* 2003; von Coelln *et al.* 2004; Perez and Palmiter 2005). We therefore speculate that HRD1 degrades Pael-R and possibly other proteins to balance the unfolded protein accumulation caused by Parkin gene mutation; nonetheless, it is possible that other unknown E3s participate in this degradation in the absence of Parkin, although the reason behind the loss of

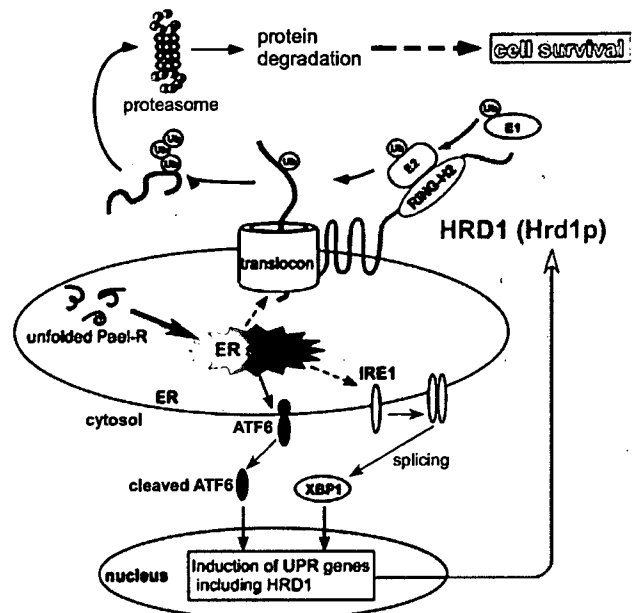


**Fig. 8** A hypothetical model demonstrating how HRD1 participates in the degradation of unfolded Pael-R. When unfolded Pael-R is accumulated in the endoplasmic reticulum, ATF6 and IRE1-XBP1 pathways are activated, and UPR genes including HRD1 are then induced. HRD1 degrades unfolded Pael-R and suppresses Pael-R-induced cell death.

dopaminergic neurons in AR-JP patients but not in Parkin knockout mice remains unknown despite the similarity in the functional loss of Parkin. On the other hand, it is likely that HRD1 ubiquitinates not only Pael-R but also other substrates related to conformational diseases caused by the accumulation of unfolded proteins as HRD1 can suppress global endoplasmic reticulum stress induced by various chemical reagents.

### Acknowledgements

We are grateful to Dr. Yuzuru Imai for his helpful discussions. We thank Otsuka GEN Research Institute for providing the HRD1 antibody. We also thank Dr. Takahiro Taira and Mr. Takanori Tabata for their helpful discussions. We thank Mr. T. Itou, Mitsubishi Chemical Safety Institute, LTD. for pertinent advices on immunohistochemical study. This study was supported by Grants-in-Aid for Scientific Research from the Ministry of Education, Culture, Sports, Science and Technology, Japan.

### References

- Amano T., Yamasaki S., Yagishita N. *et al.* (2003) Synoviolin/Hrd1, an E3 ubiquitin ligase, as a novel pathogenic factor for arthropathy. *Genes Dev.* **17**, 2436–2449.
- Conway K. A., Lee S. J., Rochet J. C., Ding T. T., Williamson R. E. and Lansbury P. T. Jr (2000) Acceleration of oligomerization, not fibrillization, is a shared property of both alpha-synuclein muta-

- tions linked to early-onset Parkinson's disease: implications for pathogenesis and therapy. *Proc. Natl Acad. Sci. U S A* **97**, 571–576.
- Cox J. S., Shamu C. E. and Walter P. (1993) Transcriptional induction of genes encoding endoplasmic reticulum resident proteins requires a transmembrane protein kinase. *Cell* **73**, 1197–1206.
- Deak P. M. and Wolf D. H. (2001) Membrane topology and function of Der3/Hrd1p as a ubiquitin-protein ligase (E3) involved in endoplasmic reticulum degradation. *J. Biol. Chem.* **276**, 10 663–10 669.
- Fang D., Wang H. Y., Fang N., Altman Y., Elly C. and Liu Y. C. (2001) Cbl-b, a RING-type E3 ubiquitin ligase, targets phosphatidylinositol 3-kinase for ubiquitination in T cells. *J. Biol. Chem.* **276**, 4872–4878.
- Friedlander R., Jarosch E., Urban J., Volkwein C. and Sommer T. (2000) A regulatory link between ER-associated protein degradation and the unfolded protein response. *Nat. Cell Biol.* **2**, 379–384.
- Fujita Y., Krause G., Scheffner M., Zechner D., Leddy H. E., Behrens J., Sommer T. and Birchmeier W. (2002) Hakai, a c-Cbl-like protein, ubiquitinates and induces endocytosis of the E-cadherin complex. *Nat. Cell Biol.* **4**, 222–231.
- Gardner R. G., Swarbrick G. M., Bays N. W., Cronin S. R., Wilhovsky S., Seelig L., Kim C. and Hampton R. Y. (2000) Endoplasmic reticulum degradation requires lumen to cytosol signaling. Transmembrane control of Hrd1p by Hrd3p. *J. Cell Biol.* **151**, 69–82.
- Gardner R. G., Shearer A. G. and Hampton R. Y. (2001) In vivo action of the HRD ubiquitin ligase complex: mechanisms of endoplasmic reticulum quality control and sterol regulation. *Mol. Cell Biol.* **21**, 4276–4291.
- Goldberg M. S., Fleming S. M., Palacino J. J. *et al.* (2003) Parkin-deficient mice exhibit nigrostriatal deficits but not loss of dopaminergic neurons. *J. Biol. Chem.* **278**, 43 628–43 635.
- Haywood A. F. and Staveley B. E. (2004) Parkin counteracts symptoms in a *Drosophila* model of Parkinson's disease. *BMC Neurosci.* **5**, 14.
- Haze K., Yoshida H., Yanagi H., Yura T. and Mori K. (1999) Mammalian transcription factor ATF6 is synthesized as a transmembrane protein and activated by proteolysis in response to endoplasmic reticulum stress. *Mol. Biol. Cell* **10**, 3787–3799.
- Hershko A. and Ciechanover A. (1998) The ubiquitin system. *Annu. Rev. Biochem.* **67**, 425–479.
- Imai Y., Soda M. and Takahashi R. (2000) Parkin suppresses unfolded protein stress-induced cell death through its E3 ubiquitin-protein ligase activity. *J. Biol. Chem.* **275**, 35 661–35 664.
- Imai Y., Soda M., Inoue H., Hattori N., Mizuno Y. and Takahashi R. (2001) An unfolded putative transmembrane polypeptide, which can lead to endoplasmic reticulum stress, is a substrate of Parkin. *Cell* **105**, 891–902.
- Itier J. M., Ibanez P., Mena M. A. *et al.* (2003) Parkin gene inactivation alters behaviour and dopamine neurotransmission in the mouse. *Hum. Mol. Genet.* **12**, 2277–2291.
- Kaneko M., Ishiguro M., Niinuma Y., Uesugi M. and Nomura Y. (2002) Human HRD1 protects against ER stress-induced apoptosis through ER-associated degradation. *FEBS Lett.* **532**, 147–152.
- Kaufman R. J. (1999) Stress signaling from the lumen of the endoplasmic reticulum: coordination of gene transcriptional and translational controls. *Genes Dev.* **13**, 1211–1233.
- Kaufman R. J., Scheuner D., Schroder M., Shen X., Lee K., Liu C. Y. and Arnold S. M. (2002) The unfolded protein response in nutrient sensing and differentiation. *Nat. Rev. Mol. Cell Biol.* **3**, 411–421.
- Kikkert M., Doolman R., Dai M., Avner R., Hassink G., van Voorden S., Thanedar S., Roitelman J., Chau V. and Wiertz E. (2004) Human HRD1 is an E3 ubiquitin ligase involved in degradation of proteins from the endoplasmic reticulum. *J. Biol. Chem.* **279**, 3525–3534.
- Kitada T., Asakawa S., Hattori N., Matsumine H., Yamamura Y., Mimosima S., Yokochi M., Mizuno Y. and Shimizu N. (1998) Mutations in the parkin gene cause autosomal recessive juvenile parkinsonism. *Nature* **392**, 605–608.
- Lee A. H., Iwakoshi N. N. and Glimcher L. H. (2003) XBP-1 regulates a subset of endoplasmic reticulum resident chaperone genes in the unfolded protein response. *Mol. Cell Biol.* **23**, 7448–7459.
- Lo Bianco C., Schneider B. L., Bauer M., Sajadi A., Brice A., Iwatsubo T. and Aebischer P. (2004) Lentiviral vector delivery of parkin prevents dopaminergic degeneration in an alpha-synuclein rat model of Parkinson's disease. *Proc. Natl Acad. Sci. U S A* **101**, 17 510–17 515.
- Mizuno Y., Hattori N. and Matsumine H. (1998) Neurochemical and neurogenetic correlates of Parkinson's disease. *J. Neurochem.* **71**, 893–902.
- Molinari M., Calanca V., Galli C., Lucca P. and Paganetti P. (2003) Role of EDEM in the release of misfolded glycoproteins from the calnexin cycle. *Science* **299**, 1397–1400.
- Murakami T., Shoji M., Imai Y., Inoue H., Kawarabayashi T., Matsubara E., Harigaya Y., Sasaki A., Takahashi R. and Abe K. (2004) Pael-R is accumulated in Lewy bodies of Parkinson's disease. *Ann. Neurol.* **55**, 439–442.
- Nadav E., Shmueli A., Barr H., Gonen H., Ciechanover A. and Reiss Y. (2003) A novel mammalian endoplasmic reticulum ubiquitin ligase homologous to the yeast Hrd1. *Biochem. Biophys. Res. Commun.* **303**, 91–97.
- Nagase T., Nakayama M., Nakajima D., Kikuno R. and Ohara O. (2001) Prediction of the coding sequences of unidentified human genes. XX. The complete sequences of 100 new cDNA clones from brain which code for large proteins in vitro. *DNA Res.* **8**, 85–95.
- Oda Y., Hosokawa N., Wada I. and Nagata K. (2003) EDEM as an acceptor of terminally misfolded glycoproteins released from calnexin. *Science* **299**, 1394–1397.
- Palacino J. J., Sagi D., Goldberg M. S., Krauss S., Motz C., Wacker M., Klose J. and Shen J. (2004) Mitochondrial dysfunction and oxidative damage in parkin-deficient mice. *J. Biol. Chem.* **279**, 18 614–18 622.
- Perez F. A. and Palmiter R. D. (2005) Parkin-deficient mice are not a robust model of parkinsonism. *Proc. Natl Acad. Sci. U S A* **102**, 2174–2179.
- Periquet M., Corti O., Jacquier S. and Brice A. (2005) Proteomic analysis of parkin knockout mice: alterations in energy metabolism, protein handling and synaptic function. *J. Neurochem.* **95**, 1259–1276.
- Petrucelli L., O'Farrell C., Lockhart P. J., Baptista M., Kehoe K., Vink L., Choi P., Wolozin B., Farrer M., Hardy J. and Cookson M. R. (2002) Parkin protects against the toxicity associated with mutant alpha-synuclein: proteasome dysfunction selectively affects catecholaminergic neurons. *Neuron* **36**, 1007–1019.
- Plempner R. K., Bordallo J., Deak P. M., Taxis C., Hitt R. and Wolf D. H. (1999) Genetic interactions of Hrd3p and Der3p/Hrd1p with Sec61p suggest a retro-translocation complex mediating protein transport for ER degradation. *J. Cell Sci.* **112**, 4123–4134.
- Shen J., Chen X., Hendershot L. and Prywes R. (2002) ER stress regulation of ATF6 localization by dissociation of BiP/GRP78 binding and unmasking of Golgi localization signals. *Dev. Cell* **3**, 99–111.
- Shimura H., Schlossmacher M. G., Hattori N., Frosch M. P., Trockenbacher A., Schneider R., Mizuno Y., Kosik K. S. and Selkoe D. J. (2001) Ubiquitination of a new form of alpha-synuclein by parkin from human brain: implications for Parkinson's disease. *Science* **293**, 263–269.

- Sidrauski C. and Walter P. (1997) The transmembrane kinase Ire1p is a site-specific endonuclease that initiates mRNA splicing in the unfolded protein response. *Cell* **90**, 1031–1039.
- Tofaris G. K., Layfield R. and Spillantini M. G. (2001) Alpha-synuclein metabolism and aggregation is linked to ubiquitin-independent degradation by the proteasome. *FEBS Lett.* **509**, 22–26.
- Travers K. J., Patil C. K., Wodicka L., Lockhart D. J., Weissman J. S. and Walter P. (2000) Functional and genomic analyses reveal an essential coordination between the unfolded protein response and ER-associated degradation. *Cell* **101**, 249–258.
- Trojanowski J. Q., Goedert M., Iwatsubo T. and Lee V. M. (1998) Fatal attractions: abnormal protein aggregation and neuron death in Parkinson's disease and Lewy body dementia. *Cell Death Differ.* **5**, 832–837.
- Von Coeln R., Thomas B., Savitt J. M., Lim K. L., Sasaki M., Hess E. J., Dawson V. L. and Dawson T. M. (2004) Loss of locus coeruleus neurons and reduced startle in parkin null mice. *Proc. Natl Acad. Sci. U S A* **101**, 10 744–10 749.
- Yang Y., Nishimura I., Imai Y., Takahashi R. and Lu B. (2003) Parkin suppresses dopaminergic neuron-selective neurotoxicity induced by Pael-R in *Drosophila*. *Neuron* **37**, 911–924.
- Ye J., Rawson R. B., Komuro R., Chen X., Dave U. P., Prywes R., Brown M. S. and Goldstein J. L. (2000) ER stress induces cleavage of membrane-bound ATF6 by the same proteases that process SREBPs. *Mol. Cell* **6**, 1355–1364.
- Yoshida H., Matsui T., Yamamoto A., Okada T. and Mori K. (2001) XBP1 mRNA is induced by ATF6 and spliced by IRE1 in response to ER stress to produce a highly active transcription factor. *Cell* **107**, 881–891.
- Zheng N., Wang P., Jeffrey P. D. and Pavletich N. P. (2000) Structure of a c-Cbl-UbcH7 complex: RING domain function in ubiquitin-protein ligases. *Cell* **102**, 533–539.

Short communication

## Heterogeneous epileptogenicity and cortical function within malformations of cortical development: A case report

Masako Kinoshita<sup>a</sup>, Akio Ikeda<sup>a</sup>, Junya Taki<sup>b</sup>, Keiko Usui<sup>c</sup>, Riki Matsumoto<sup>a</sup>,  
Nobuhiro Mikuni<sup>b</sup>, Jun B. Takahashi<sup>b</sup>, Hidenao Fukuyama<sup>c</sup>,  
Nobuo Hashimoto<sup>b</sup>, Ryosuke Takahashi<sup>a</sup>

<sup>a</sup> Department of Neurology, Graduate School of Medicine, Kyoto University, 54 Shogoin-Kawaharacho, Sakyo, Kyoto, 606-8507, Japan

<sup>b</sup> Department of Neurosurgery, Graduate School of Medicine, Kyoto University, 54 Shogoin-Kawaharacho, Sakyo, Kyoto, 606-8507, Japan

<sup>c</sup> Human Brain Research Center, Graduate School of Medicine, Kyoto University, 54 Shogoin-Kawaharacho, Sakyo, Kyoto, 606-8507, Japan

Received 30 December 2005; received in revised form 19 July 2006; accepted 11 September 2006

Available online 13 November 2006

### Abstract

The authors report a 24-year-old patient with intractable partial epilepsy and massive malformations of cortical development (MCD). Subdural EEG recordings of habitual seizures showed heterogeneous epileptogenicity, and visual evoked potential was recorded within the MCD just adjacent to the most active epileptogenic focus. Resection of the small cortical area presumably with core epileptogenicity, while sparing the cortical functional area, improved seizure outcome without any postoperative functional deficits.

© 2006 Elsevier B.V. All rights reserved.

**Keywords:** Epileptogenicity; Cortical function; Malformations of cortical development; Visual evoked potential; Subdural EEG record; Epilepsy surgery

### 1. Introduction

Malformations of cortical development (MCDs) are present in 15–20% of adult patients with intractable partial epilepsy [1]. However, epileptogenicity within MCD varies within as well as among individuals: epileptic activities correlate with in situ histopathologic patterns in MCD [2]. Several case reports have suggested a possibility that partial resection of MCD can give a good seizure outcome [3,4] although generally the best seizure control has been achieved when complete or major excision of both the MRI-visible lesion and the cortical areas generating ictal electrographic activity [4,5]. Recent case reports and imaging studies have shown that cortices showing MCD have normal brain functions [6–9], and therefore, resection of MCD may carry a potential risk of neurological functional deficits.

Here we report a patient with partial seizures caused by MCD which had heterogeneous epileptogenicity and visual function delineated by presurgical evaluation using subdural electrodes. The most active epileptogenic area and visual functional area resided side by side within MCD. After resection of the small area of the most active epileptogenicity, the seizures significantly decreased with no functional deficits in spite of large residual MCD.

### 2. Patient and methods

#### 2.1. Case presentation

A 24-year-old right-handed woman with medically intractable partial seizures had implanted subdural electrodes for presurgical evaluation. All the clinical procedures were done after full explanation about the methods and possible side effects to the patient and her family, according to clinical research protocol approved by the Ethical Committee of

Corresponding author. Tel.: +81 75 751 3772; fax: +81 75 751 9416.

E-mail address: akio@kuhp.kyoto-u.ac.jp (A. Ikeda).

Kyoto University Graduate School of Medicine (No. 79). She developed complex partial seizures (CPSs) when she was 17 years old. Her habitual seizures started with auras consisting of a sensation that something was rising from her feet and/or auditory hallucination of high-pitched sound, developed to CPSs with oral (chewing) and bilateral hand automatisms, followed by postictal cough. She had no personal or familial antecedents for epilepsy. Neurological examination showed left lower homonymous quadrantanopsia. Her seizures were intractable in spite of administration of multiple drugs such as phenytoin, carbamazepine, phenobarbital and clobazam of appropriate dose.

An MRI revealed massive MCDs including schizencephaly and polymicrogyria in the right temporo-parieto-occipital area (Fig. 1A–D). By non-invasive video-EEG monitoring during habitual seizures consisted of motion arrest, staring, oral and hand automatisms, ictal discharges started with low-voltage fast activities at the right posterior temporal area before the clinical onset. Interictal FDG-PET showed heterogeneous regional glucose hypometabolism in the right temporo-occipital area (Fig. 1E), and ictal SPECT

showed an increased perfusion in that area (Fig. 1F). Intra-carotid propofol test [10] revealed language and memory dominance in the left hemisphere.

## 2.2. Presurgical evaluation with subdural electrodes

The electrodes were disks of 3.0 mm diameter made of platinum–iridium (Ad-Tech, Racine, WI, U.S.A.), placed with center-to-center distance of 1 cm within the silicon rubber sheet. Two sheets of 4 × 5 subdural electrode grid, one each on the right parietal and temporal lobes, and one 1 × 4 subdural electrode strip on the right temporal lobe were implanted. One set of depth electrodes made of platinum, 1.5 mm diameter, 4-contact of 1.0 mm length, with 5 mm spacing (UNIQUE MEDICAL, Tokyo, Japan), was inserted into the right antero-temporal area. The epileptogenic area was determined by simultaneous monitoring of video and subdural EEG during the patient's habitual clinical seizures.

Functional mapping was performed with the left median and tibial somatosensory evoked potential (SEP), auditory evoked potential (AEP) and visual evoked potential (VEP)

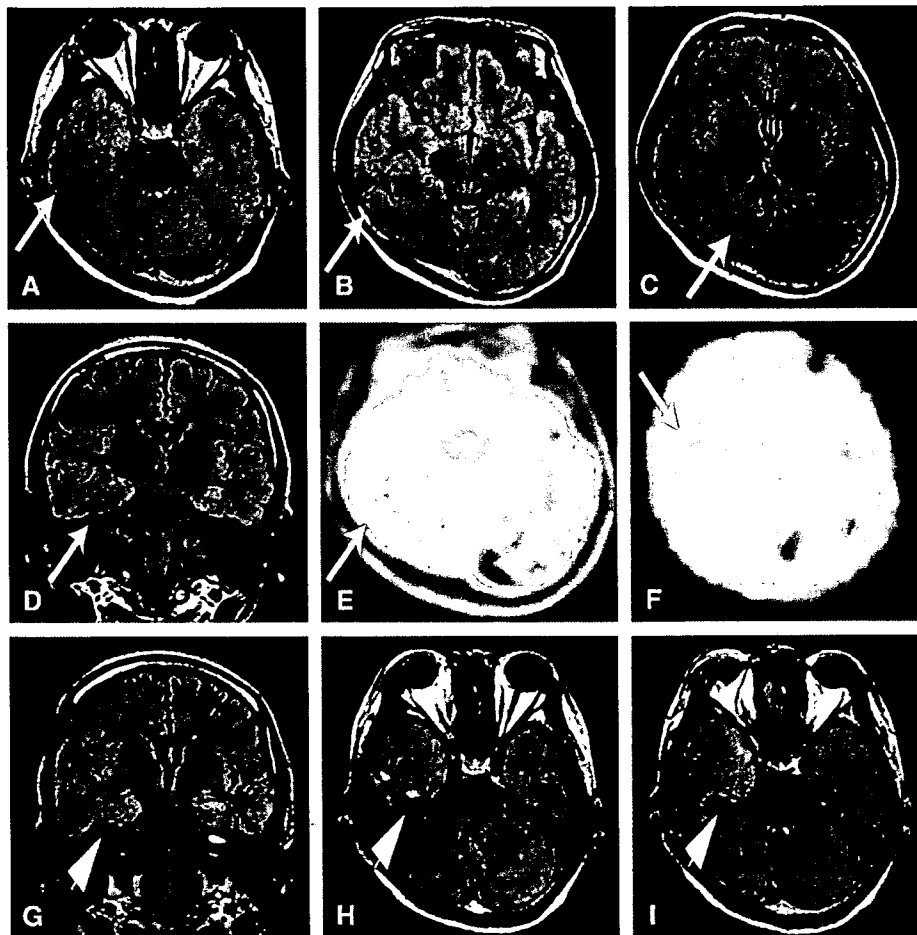


Fig. 1. Preoperative brain MRI (A–D), interictal FDG-PET (E), ictal SPECT (F) and postoperative brain MRI (G–I). (A–D) Massive MCD including a schizencephaly and polymicrogyria in the right temporo-parieto-occipital area (arrows). (E) Heterogeneous regional glucose hypometabolism in the right temporo-occipital area. (F) Ictal SPECT showed an increased perfusion in that area. (G–I) Small area with the most active epileptogenicity was resected (arrowhead). The patient showed reduction of seizures (Engel's class IIA) in spite of a large residual lesion.

studies and electric cortical stimulation. Electric cortical stimulation was performed using 50 Hz, bipolar, alternating square pulse of 0.3 ms duration.

### 3. Results

#### 3.1. Delineation of epileptogenic area

She had five CPSs during the invasive monitoring period, and none of them were preceded by her typical aura. Subdural EEG showed that three seizures started with low-voltage fast activities in the posterior part of the right mesial temporal area (bold circles, Fig. 2A) followed by burst of spikes, and then spread to the lateral part. Clinical manifestation of one of them consisted of motion arrest followed by oral and bilateral hand automatisms, and the other two showed motion arrest only. One seizure with motion arrest started with low-voltage fast activities at one electrode (C4, shaded circle in Fig. 2A) in the anterior lateral temporal area, spread to basal temporal area showing rhythmic spikes. The other seizure with motion arrest and oral and bilateral hand automatisms started with spikes in the posterior part of the right lateral electrodes (A6 and A11, oblique lines in Fig. 2A). Additionally she had two habitual auras during invasive monitoring, but no EEG

changes occurred. Interictal spikes were frequently seen in the mesial side of the posterior basal temporal area, and quickly spread to the adjacent electrodes (Fig. 2B and C).

#### 3.2. Functional mapping

Pattern-reversal, visual stimulation of the fovea ( $3^\circ \times 3^\circ$ ) and central visual field ( $10^\circ \times 10^\circ$ ) evoked responses in the basal temporal area adjacent to the most active epileptogenic focus (Fig. 3). Left peripheral hemifield stimulation elicited evoked potentials in the more mesial area, while no responses were seen to the right peripheral hemifield stimulation. Median and tibial SEP and AEP showed non-primary responses at the electrodes located on the lateral superior temporal areas. Electric cortical stimulation at the basal temporal electrodes in the vicinity of the area where VEP was evoked elicited elementary and complex hallucinations in the left upper visual field in the absence of afterdischarges or her habitual auras (Fig. 4).

#### 3.3. Surgical outcome and seizure control

The most active epileptic region in the right mesial basal temporal area within the MCD was resected tailored by

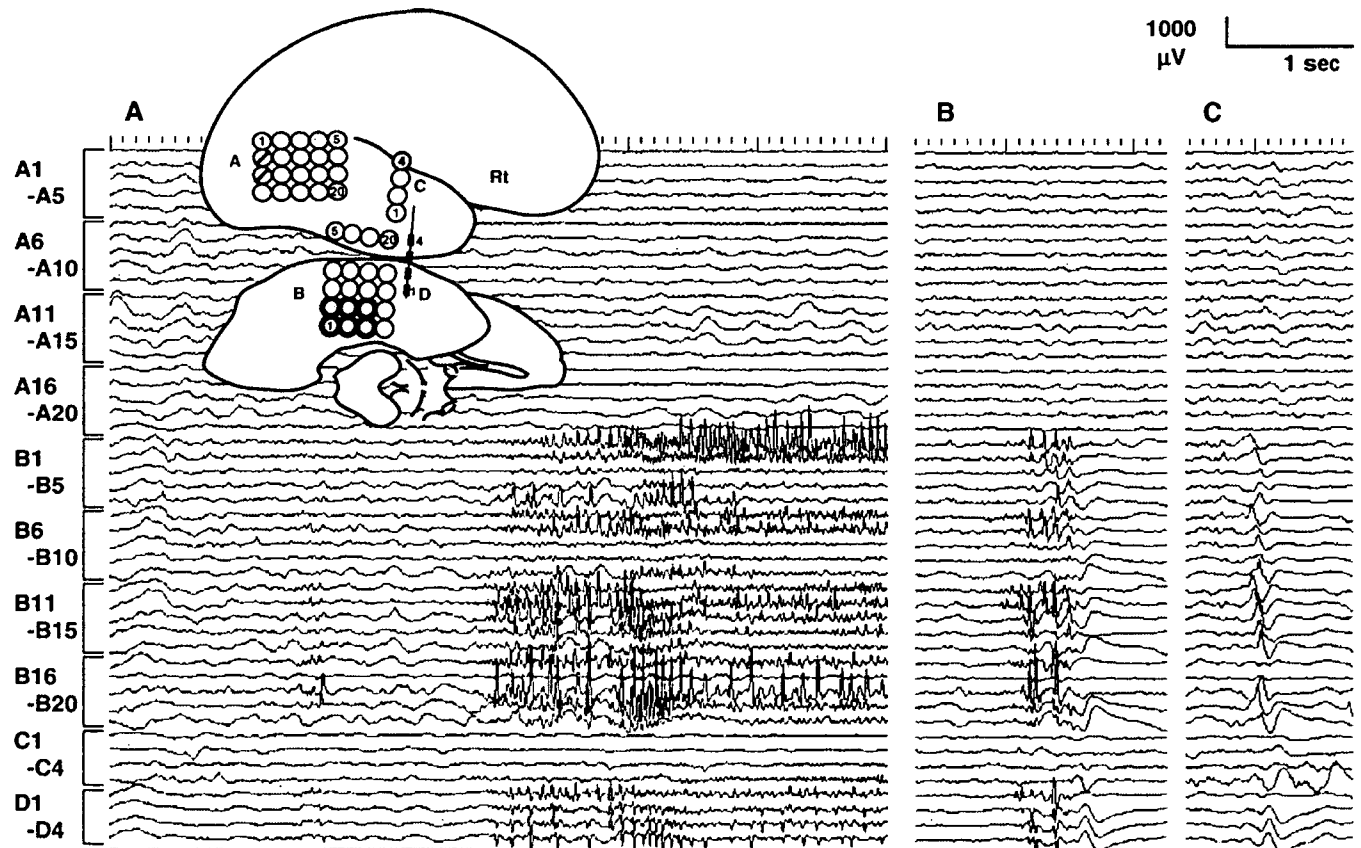


Fig. 2. Invasive EEG records. (A) Recording of a habitual seizure. Electrographic seizures most frequently started from the posterior part of the right mesial temporal area (bold circles, subdural record) approximately 15 s before the clinical onset; these areas were resected. A shaded circle and circles with oblique lines indicate other epileptogenic foci with lesser activity. (B, C) Interictal record. Interictal spikes were frequently seen in the mesial side of the posterior basal temporal area, and easily spread to the adjacent electrodes.



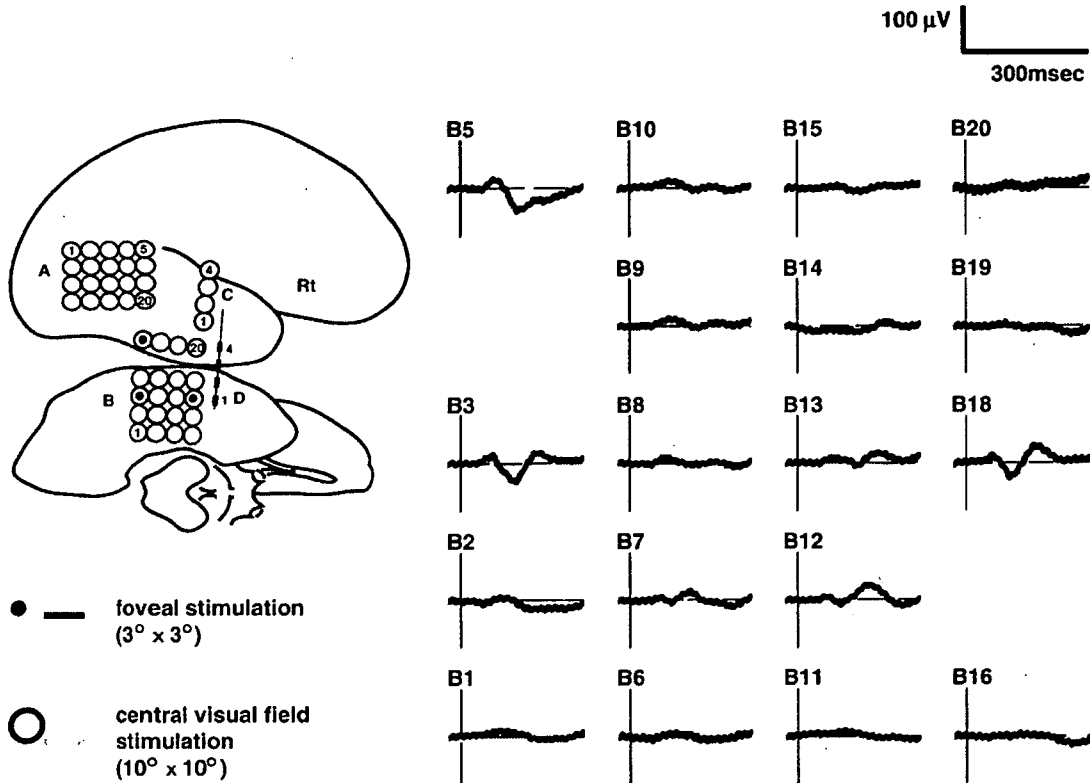


Fig. 3. VEP recording in the right basal temporal area (B plate). Foveal (dots, thick lines) and central visual field stimulation (shaded circles, gray lines) elicited responses adjacent to the most active epileptogenic area. Epilepsy surgery was performed with the best effort to spare the functional area as much as possible.

invasive EEG using subdural and depth electrodes (Figs. 1G–I and 2A) with the best effort to spare the functional area as much as possible. Histological diagnosis of the resected

epileptogenic area of the patient was type IA cortical dysplasia without any balloon cells (BCs). The patient developed no neurological deficits after resection. During

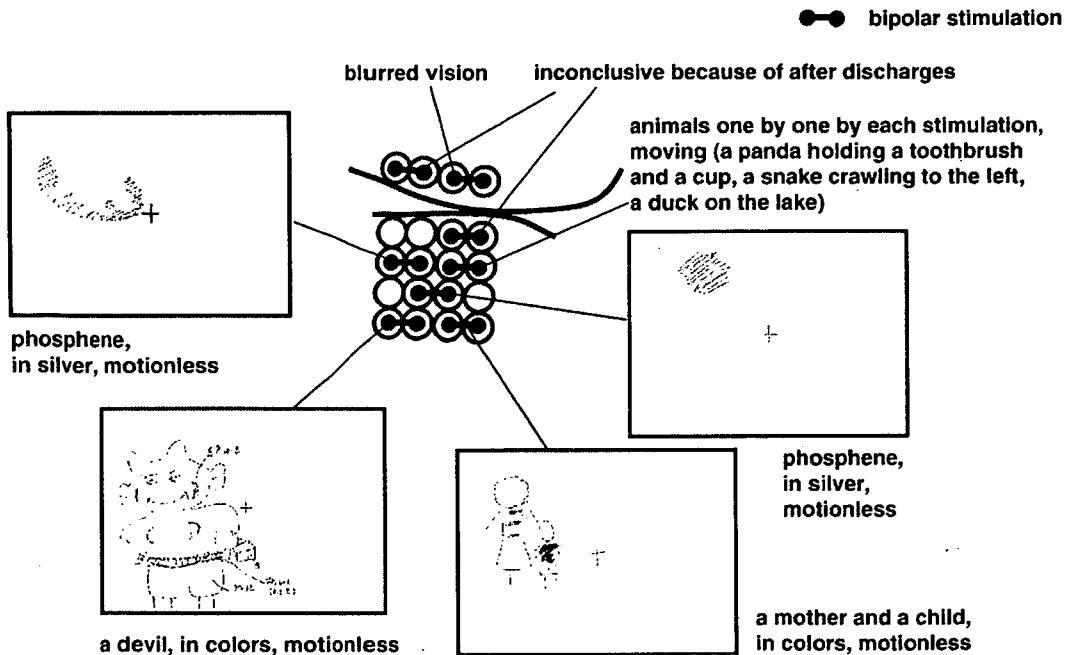


Fig. 4. Electric cortical stimulation at the basal temporal electrodes in the vicinity of the area where VEP was evoked (B plate, see Fig. 3). Elementary and complex hallucinations were elicited in the left upper visual field. Reproducibility of the symptoms was confirmed in the absence of afterdischarges or auras (insets are patient's own drawings of what she saw during stimulation).

two months after surgery the patient developed non-epileptic auditory hallucination consisting of the feeling that somebody was always talking to and chasing her, and they were totally different from her habitual auras. Before surgery, the patient had experienced the similar symptom only twice. This psychotic event was successfully controlled by neuroleptic medication of risperidone and olanzapine, therefore we consider it as post operative psychosis associated with forced normalization [11]. After a follow-up period of 2 years, the patient was in Engel's class IIA.

#### 4. Discussion

This case demonstrated the presence of heterogeneous epileptogenicity within MCD by means of invasive EEG recording. Invasive EEG findings during habitual seizures and of interictal period suggested multiple foci within the lesion, and the most active epileptogenic region was found in the mesial side of the right basal temporal area, whose histopathology showed a mild cortical dysplasia without any BCs. The present finding is in accordance with a previous report which demonstrated, within individual MCD, that dysplastic lesions containing BCs (type IIB) were less epileptogenic than those without BCs (type I and type IIA) [2].

VEP in the present patient demonstrated that the MCD lesion in the basal temporal area participated in visual processing. In this patient, high-amplitude cortical potentials were elicited by central, foveal and left peripheral hemifield stimulation but not by right peripheral hemifield stimulation, suggesting that this cortical area possessed the function of the primary visual cortex. However, the broad distribution of VEP with the most prominent potentials in the mesial part of basal temporal area differed from the well-known, strict localization of high-amplitude responses [12]. This difference is possibly explained by atypical organization of cortical function in the present patient, as shown in previous PET and functional MRI studies [6,7]. Moreover, this patient showed elementary and complex visual hallucinations when the basal temporal area was stimulated. Elementary hallucinations occur with the involvement of the primary visual cortex [13], and thus if they were observed during spontaneous temporal lobe seizures or upon electrical stimulation of the temporal lobe, usually they were explained by the spread of activity to the occipital lobe [13]. Therefore, elementary hallucinations in this patient produced by electric stimulation suggest the atypical location of the primary visual cortex in the basal temporal area.

In summary, this case report demonstrated that the seizure reduction with sparing the functional area can be achieved by precise presurgical evaluation using subdural electrodes, including electric cortical stimulation, recordings of habitual

seizures and evoked potentials. More case accumulation is warranted to prove the notion that it is possible to achieve not only the maximum seizure reduction but also the minimum functional deficits by epilepsy surgery.

#### Acknowledgment

The authors thank Dr. Akira Sengoku, Sengoku clinic, Kyoto-shi, Japan, for referring the patient. This study was supported by the Research Grant for the Treatment of Intractable Epilepsy (16-1) from the Japan Ministry of Health, Labour and Welfare, and Scientific Research Grant (C2) from the Japan Society for Promotion of Science (JSPS).

#### References

- [1] Kuzniecky RI, Jackson GD. Developmental disorders. In: Engel Jr J, Pedley TA, editors. *Epilepsy A Comprehensive Textbook*. Philadelphia: Lippincott-Raven; 1997, p. 2517–32.
- [2] Boonyapisit K, Najm I, Klem G, Ying Z, Burrier C, LaPresto E, et al. Epileptogenicity of focal cortical malformations due to abnormal cortical development: direct electrocorticographic–histopathologic correlations. *Epilepsia* 2003;44(1):69–76.
- [3] Francione S, Vigliano P, Tassi L, Cardinale F, Mai R, Lo Russo G, et al. Surgery for drug resistant partial epilepsy in children with focal cortical dysplasia: anatomical–clinical correlations and neurophysiological data in 10 patients. *J Neurol Neurosurg Psychiatry* 2003;74:1493–501.
- [4] Chassoux F, Devaux B, Landré E, Turak B, Nataf F, Varlet P, et al. Stereoelectroencephalography in focal cortical dysplasia. A 3D approach to delineating the dysplastic cortex. *Brain* 2000;123:1733–51.
- [5] Palmieri A, Gambardella A, Andermann F, Dubeau F, da Costa JC, Olivier A, et al. Operative strategies for patients with cortical dysplastic lesions and intractable epilepsy. *Epilepsia* 1994;35:S57–71.
- [6] Janszky J, Ebner A, Kruse B, Mertens M, Jokeit H, Seitz RJ, et al. Functional organization of the brain with malformations of cortical development. *Ann Neurol* 2003;53:759–67.
- [7] Richardson MP, Koepp MJ, Brooks DJ, Coull JT, Grasby P, Fish DR, et al. Cerebral activation in malformations of cortical development. *Brain* 1998;121:1295–304.
- [8] Innocenti GM, Maeder P, Knyazeva MG, Fomari E, Deonna T. Functional activation of microgyric visual cortex in a human. *Ann Neurol* 2001;50:672–6.
- [9] Mikuni N, Ikeda A, Yoneko H, Amano S, Hanakawa T, Fukuyama H, et al. Surgical resection of an epileptogenic cortical dysplasia in the deep foot sensorimotor area. *Epilepsy Behav* 2005;7:559–62.
- [10] Takayama M, Miyamoto S, Ikeda A, Mikuni N, Takahashi JB, Usui K, et al. Intracarotid propofol test for speech and memory dominance in man. *Neurology* 2004;63:510–5.
- [11] Andermann LF, Savard G, Meencke HJ, McLachlan R, Moshe S, Andermann F. Psychosis after resection of ganglioglioma or DNET: evidence for an association. *Epilepsia* 1999;40:83–7.
- [12] Noachtar S, Hashimoto T, Lüders H. Pattern visual evoked potentials recorded from human occipital cortex with chronic subdural electrodes. *Electroencephalogr Clin Neurophysiol* 1993;88:435–46.
- [13] Bien CG, Benninger FO, Urbach H, Schramm J, Kurthen M, Elger CE. Localizing value of epileptic visual auras. *Brain* 2000;123:244–53.

特集 パーキンソン病の診断と治療の進歩

## パーキンソン病の分子病態

高橋良輔 王華芹

別刷

日本医師会雑誌

第135巻・第1号

平成18(2006)年4月

# パーキンソン病の分子病態

高橋良輔\* 王 華芹\*\*

キーワード パーキン パエル受容体 小胞体ストレス 酸化的ストレス

## はじめに

パーキンソン病 (PD) は老年者に罹患率の高い神経変性疾患である。臨床症状として、振戦、固縮、無動、姿勢歩行障害などがみられる。病理学的には中脳黒質のドパミン神経の選択的変性脱落および細胞内封入体(レビー小体)の形成を特徴とする。ミトコンドリア機能異常、酸化的ストレスおよび蛋白質分解異常が主な原因として指摘されているが、選択的なドパミン神経細胞死の原因はいまだに明らかになっていない。

PD の多くは孤発性であるが、その一部は家族性・遺伝性に発症する。遺伝学、分子生物学の発展を追い風に、遺伝性 PD からの PD 発症機構解明のアプローチが盛んになり、家族性 PD の原因遺伝子が相次いでクローニングされてきた。現在、PARK1~11, NR4A2 を含めて 12 の遺伝子座が特定され、そのうち  $\alpha$ -シヌクレイン ( $\alpha$ -synuclein, PARK1), パーキン (*parkin*, PARK2), *UCH-L1* (PARK5), *PINK1* (PARK6), *DJ-1* (PARK7), *LRRK2* (PARK8) および *Nurr1* の 7 つの遺伝子が単離されている。

これらの遺伝子同定および機能解析は単なる家族性 PD のみならず、より一般的な孤発性 PD の病態解明につながる可能性が期待されている。

る。たとえば、酸化的ストレスと蛋白質分解異常は孤発性 PD の病因因子として古くから指摘されてきた。パーキンは数多くあるユビキチンリガーゼ (E3) の 1 つに位置付けられ、ミスフォールド化した異常蛋白質の蓄積が PD の病因仮説として有力になっている。この発見は家族性 PD が孤発性 PD と共通の病的機序を有することを示唆し、家族性 PD 原因遺伝子の機能解析が孤発性 PD の病態メカニズムを理解する手がかりとなることが予想される。

## I. パーキンは E3 である

パーキンは日本人家系から常染色体劣性遺伝性若年性パーキンソニズム (AR-JP) の原因遺伝子として同定された<sup>1)</sup>。その後、パーキン遺伝子変異の報告は世界中でなされており、遺伝子の部分欠失をはじめとし、部分重複、ナンセンス、ミスセンス、および挿入変異など、遺伝子全長を通じてさまざまな変異の報告がある。遺伝性 PD において、一般に遺伝子変異がきわめて頻度が低いのに対し、パーキンが原因となる場合は比較的多く、劣性遺伝性で、しかも若年性発症であれば約半数にパーキン遺伝子の変異が観察される。

パーキンの遺伝子産物はアミノ酸 465 個からなり、N 末端にユビキチン様領域 (Ubl), C 末端にはリングフィンガーモチーフ (RING finger motif) を 2 個、そしてユビキチン様領域とリングフィンガーモチーフをつなぐリンカー領域より構成されている。リングフィンガーモチーフ

\*たかはし・りょうすけ：京都大学大学院医学研究科教授 (臨床神経学)。

昭和 58 年京都大学医学部卒業。

主研究領域/ALS とパーキンソン病の分子生物学。

\*\*おう・かきん：京都大学大学院医学研究科先端領域融合医学研究機構特任助手。